https://doi.org/10.5194/egusphere-2022-122
Preprint. Discussion started: 11 April 2022

Evaluating the applicability of a terrain-based floodplain delineation tool for a broad-scale assessment of flood exposure of tailings deposits

Gabriel Pérez-Murillo[1], Neil. McIntyre[1], Raymond C. Z. Cohen[2] and Mahesh Prakash[2]

[1]Centre for Water in the Minerals Industry, Sustainable Minerals Institute, The University of Queensland, Brisbane QLD 4072, Australia
[2]Data61, CSIRO, Clayton, VIC 3168, Australia

Correspondence to: G. Pérez-Murillo (g.perezmurillo@uq.edu.au)

Abstract. Construction and abandonment of mine tailings deposits in river floodplains have created environmental risks associated with the release of toxic substances during floods. Assessment tools are needed to understand levels of risk and to prioritize sites for management. These tools need to be computationally efficient over wide areas, potentially whole river basins, which generally excludes reliance on 2D hydrodynamic models. This research evaluates the applicability of a terrain-based floodplain delineation tool (GFPLAIN) to assess flood exposure of tailings deposits by comparing its results against a 2D hydrodynamic model, the Shallow Water Integrated Flood Tool (SWIFT). For this compassion, the case study area of Copiapó River Basin (Atacama, Chile) was used to model two flood scenarios, the extreme flood event of March 2015, and a hypothetical flood with a 100-year return period. Overall, the GFPLAIN flood maps showed limitations in reproducing the list of tailings deposits identified as exposed by SWIFT, with some agreement between some of the top 10 deposits prioritized by these tools. We conclude that GFPLAIN, while fast to apply and potentially able to prioritize sites at risk, has limitations in providing an accurate and complete assessment due to its limited consideration of local terrain and flood dynamics.

1 Introduction

Floods are the most common natural hazard, and their frequency and devastating effects are likely to increase due to climate change and land-use intensification (Merz et al., 2014; Alfieri et al., 2015; Tabari, 2020). Mining is one industry for which floods can generate economic loss and environmental degradation due to impacts on operations and releases of contaminated water from mine sites (Banwart et al., 2002; Eisler and Wiemeyer, 2004). For example, the extreme flood events between 2007 and 2011 in Queensland (Australia), accrued losses of more than $2 billion in export earnings derived from mining (Sharma and Franks, 2013). Consequently, the quantification of economic and environmental risks associated with floods have received increasing attention by the mining industry and regulators over the last decade (Pearce et al., 2011; Gonzalez et al., 2019).

Of particular public concern, flooding of mined land can have a long-lasting impact on ecosystems due to the spread of pollutants released from mine wastes such as tailings (Foulds et al., 2014; Pavlowsky et al., 2017; Kincey et al., 2018). The term “tailings” has been used to describe mining waste produced as a by-product of mineral processing (Blight, 2011; Kossoff et al., 2014). Tailings can contain high concentrations of hazardous pollutants such as arsenic (Liu et al., 2010), cyanide

https://doi.org/10.5194/egusphere-2022-122
Preprint. Discussion started: 11 April 2022

(Donato et al., 2007; Bakatula and Tutu, 2016), heavy metals (Lottermoser, 2010; Johnson et al., 2016) and, depending on the extracted commodity, even traces of radioactive elements (Landa 2004; Winde and van der Walt, 2004). Tailings can be found as an unprotected pile of sand-like material commonly referred to as Legacy Tailings Deposits (LTDs). These LTDs commonly lack ownership, protective capping layers and adequate infrastructure to protect them against erosion, thus posing a long-lasting environmental hazard especially those LTDs that sit on a flood plain (Navarro et al., 2008; Martín-Duque et al., 2015; Kincey et al., 2018). On the other hand, most modern mining operations store tailings in engineered impoundment structures commonly refered to as Tailings Storage Facilities (TSFs), which pose a lesser environmental risk when constructed and managed under the recent industry standards and best practice guidelines (ANCOLD,2003; Ministerio de Mineria 2007; CDA, 2013; ICMM, 2016).

When floodwaters reach unprotected tailings deposits, tailings particles can be saturated or eroded, which can lead to dissolution and transport of harmful substances into surface waters (Concas et al., 2006; Castro-Bolinaga et al., 2015). Tailings-borne pollutants can travel in surface waters as suspended particles or dissolved species (Andrade et al., 2006), reaching crops (Grimalt et al., 1999; Mileusnić et al., 2014), humans (Ngole-Jeme and Frantke, 2017; Fei et al., 2017), and other living organisms in nearby ecosystems (Nriagu et al., 1998; Boening, 2000; Kiser et al., 2010). Although interactions between individual tailings deposits and climatic forces are often complex and site specific (Northey et al., 2017), understanding the risks derived from flood-tailings interactions over large spatial scales is necessary for prioritizing areas where mitigation actions are required. There are different examples of research focused on the prioritization of tailings deposits to reduce environmental pollution risks or mitigate potential impacts on human health (e.g Mhlongo, et al., 2019; Mitchell et al., 2019; Lam et al., 2020). However, none of these studies has focused on assessing the risk chain derived from flood erosion of tailings deposits. For this reason, this research focuses on evaluating the first link in this chain of risks; flood exposure assessment of tailings deposits, choosing as a case study region a river basin with historical mining and dozens of tailings deposits located along the main river floodplains.

In the general context of flood risk management, the risk assessment process starts by identifying flood prone areas and quantifying flood hazards through the delineation of flood maps (Schanze, 2006; European Council, 2007; Environment Agency, 2014). Currently, there are multiple alternatives to delineate flood maps and estimate flood related magnitudes such as flood height, flood velocity, and inundation times (Néelz and Pender, 2013; Jain et al., 2018; Nkwunonwo et al., 2020). Commonly, 2D-hydrodynamic models are considered the industry standard for flood risk studies since they have the highest potential for being accurate over a range of floods (Teng et al., 2017). However, in areas with sparse hydrologic data and a lack of high-resolution terrain data, it is often not feasible or not useful to implement a hydrodynamic model over a large spatial scale such as an entire river basin. Therefore, recent publications have proposed simplified alternatives to hydrodynamic models, which vary substantially in their level of complexity, intended application, hydraulic assumptions, data requirements and computational demand (e.g., White et al., 2012; Clubb et al., 2017; Afshari et al., 2018; Zheng et al., 2018 Jafarzadegan et al., 2018; Bernhofen et al., 2018; Nardi et al., 2019). Despite their dissimilarity, a group of these techniques can be broadly

https://doi.org/10.5194/egusphere-2022-122
Preprint. Discussion started: 11 April 2022

classified under the label of "terrain-based" flood mapping tools, since their main input is terrain data in the form of a Digital Elevation Model (DEM) or a Digital Terrain Model (DTM). The main characteristic of these tools is their use of geomorphologic classification procedures implemented through Geographic Information Systems (GIS) for a fast identification of flood prone areas (Samela et al., 2018). The use of terrain-based flood mapping tools is further justified at large spatial scales, considering that both terrain-based and hydrodynamic models yield floodplain predictions with considerable uncertainties (Sampson, et al., 2015; Motevalli and Vafakhah, 2016). An alternative to computer modelling for flood hazard assessment is to use existing maps with national and regional flood hazard evaluation associated with certain pre-defined return periods (e.g., Environment Agency, 2019; FEMA, 2021). However, these maps rarely exist in remote historical mining regions, which makes it of special interest to evaluate the applicability and usefulness of simplified alternatives such as terrain-based tools.

This research aims to answer the question of how adequate is a terrain-based floodplain delineation tool is, implemented based on moderate resolution terrain data, for assessing flood exposure of tailings deposits at a river basin scale? This question was addressed through the comparison of the flood maps obtained with a modified version of the Geomorphological Floodplain delineation algorithm (GFPLAIN) against the detailed flood maps obtained with a 2D hydrodynamic model; the Shallow Water Integrated Flood Tool (SWIFT), for the case study region of Copiapó River Basin (Atacama, Northern Chile).Since the applicability of the terrain-based tool is focused on the evaluation of exposure of tailings deposits, this comparison between models was made through flood exposure metrics, rather than the traditional flood mapping performance metrics. In Section 2, the reader will be introduced to the case study region, the modelling tools, the flood assessment methodology, and the methods for inter-comparison between the results obtained with these models. The results of the models' evaluation are presented in Section 3, while Section 4 and Section 5 will present the discussion and the conclusions respectively.

2 Materials and methods

2.1 Case study area

Copiapó River Basin has an approximate area of 18,700 km^2 and is located in the southern part of Atacama Desert at the Atacama Region of Northern Chile (Fig. 1a). The average annual precipitation registered in this river basin is 31 mm (Climate-Data.org, 2021), with a predominantly semi-arid climate according to the Köppen-Geiger classification (Sarricolea et al., 2017). The main surface streams draining this river basin are the Copiapó river, and Quebrada Paipote (Claro et al., 2018). The flow estimation points for these streams, used later as flow inputs for SWIFT, are represented as crosses in Fig. 1b. The main economic activities in this region are agriculture, focusing on grape and olive tree cultivation, and mining of copper and gold deposits (ODEPA, 2019). Mining has existed in this region for more than 200 years, resulting in the construction of more than 118 tailings deposits, from which 23 can be classified as modern currently active TSFs, 88 as inactive deposits of different configurations and 7 as abandoned deposits or LTDs (see Fig.1a).

https://doi.org/10.5194/egusphere-2022-122
Preprint. Discussion started: 11 April 2022

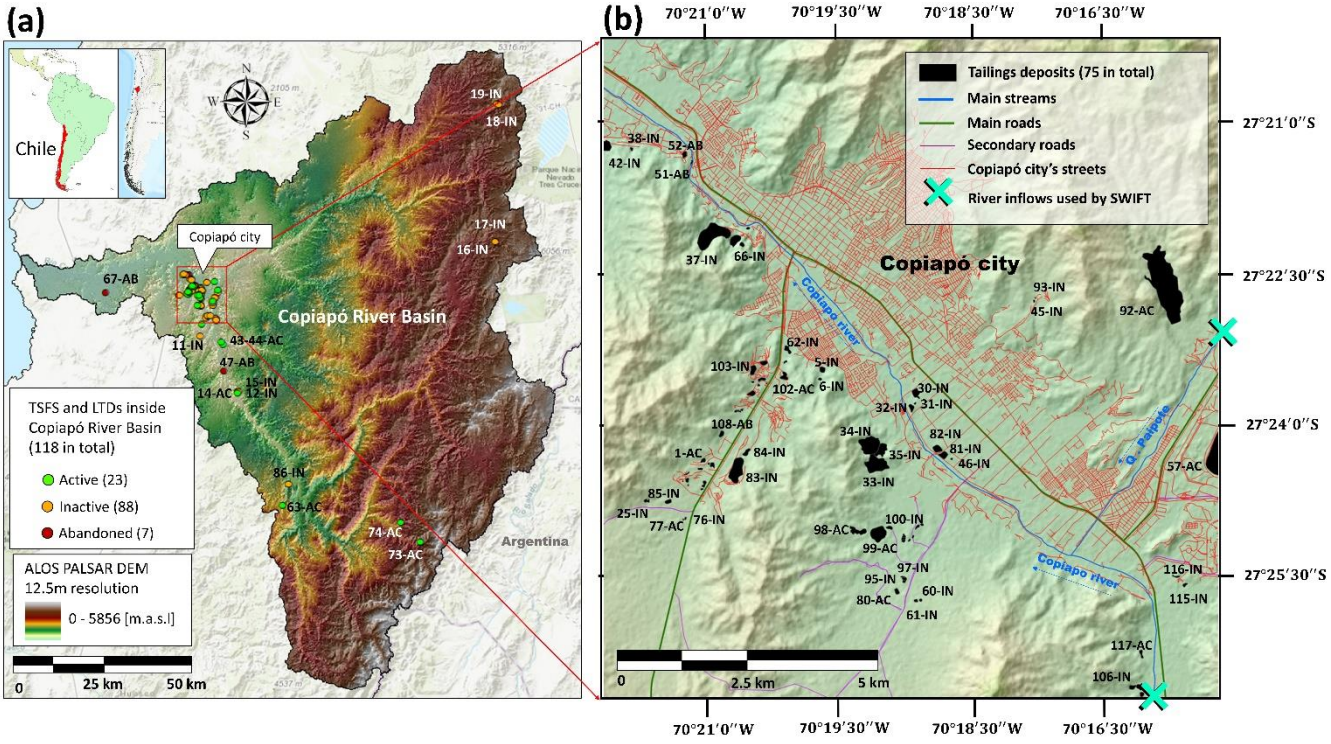

Figure 1.(a) Location of Copiapó River Basin and location of tailings deposits as reported by Servicio Nacional de Geología y Minería or SERNAGEOMIN for its initials in Spanish (SERNAGEOMIN, 2020). Background image: topographic basemap provided by Esri 2021. **(b)** Intercomparison extent with locations of deposits' polygons labelled according to operational status (Active: AC, Inactive: IN, and Abandoned: AB). The deposits' polygons were delineated based on satellite imagery provided by Esri, 2021, and the coordinates of each deposit provided by SERNAGEOMIN, 2020. DEM used in these maps corresponds to ALOS-Palsar RTC product (JAXA/METI-ASF, 2007).

The model intercomparison was carried out in a rectangular area of 138 km^2, located between 70°150'–70°250' W and 27°180'–27°260' S, and comprising Copiapó city and the peri-urban areas of Paipote and Tierra-Amarilla (see Fig. 1b). This region was selected since it has experienced recent extreme flood events including that which occurred between the 24th and the 28th of March 2015 (Izquierdo et al., 2016; Valdés-Pineda et al., 2017). This modelling extent coincides with that of the implementation of SWIFT by Claro et al. (2018), used to reproduce the event of March 2015. This modelling extent also overlaps with those of previous publications focusing on environmental pollution and its relationship with mine wastes (Carkovic et al., 2016; Falcón et al., 2017; Izquierdo et al 2020), and publications focusing on flood modelling and evaluation of damages caused by the catastrophic flood event of March 2015 (Valdés-Pineda et al., 2017 and Izquierdo et al., 2021). The modelling extent contains 63% of all the tailings deposits inside Copiapó River Basin (75 out of 118). Most of these correspond to inactive tailings deposits, scattered throughout the fluvial floodplain and two other alluvial valleys align to main roads connecting to the southeast of Copiapó city (see Fig. 1b).

https://doi.org/10.5194/egusphere-2022-122
Preprint. Discussion started: 11 April 2022

2.2 Modelling tools

2.2.1 Shallow Water Integrated Flood Tool

Shallow Water Integrated Flood Tool (SWIFT) has been selected as a benchmark to evaluate the performance of the terrain-based flood mapping tool. SWIFT is a hydrodynamic model and flood mapping tool based on the 2D Shallow Water Equations. SWIFT has been benchmarked against different well-known flood inundation tools, showing good performance for modelling different critical aspects of flooding including surface flooding in urban areas, flooding of river valleys, good representation of flood propagation over an extended floodplain, and good representation of flooding due to rainfall (Cohen et al., 2016). As such, SWIFT represents the accepted, best practicable approach to flood mapping where high-resolution terrain data and flood observations are available and when computational costs and technical expertise needed for conducting a detailed flood study are not a constraint. It is also a suitable benchmark because it has been previously calibrated and validated in the case study area by Claro et al. (2018).

SWIFT implements a GPU-based solution of the 2D Shallow Water Equations using a finite-volume formulation as described by Cohen et al. (2015). It includes momentum terms for convective and advective acceleration, gravity, roughness, and water pressure. Additionally, SWIFT also accounts for time-varying boundary conditions, spatially varying floodplain roughness and the representation of complex terrain and channel features such as bridges, levees, and buildings (Hilton et al., 2015; Prakash et al., 2015). Further technical specifications are available in Cohen et al. (2015) and Cohen et al. (2016).

2.2.2 Terrain-based tool for floodplain delineation

The terrain-based tool used in this study is an adaptation of the Geomorphological Floodplain delineation algorithm (GFPLAIN) proposed by Nardi et al., (2006). This tool was selected due to its simplicity, computational efficiency, the availability of its source code and the flexibility of adaptation of its calibration methodology. Additionally, this tool has performed well compared to other GIS terrain-based floodplain delineation tools (Annis et al., 2019). GFPLAIN has also been benchmarked against national awareness maps (Nardi et al., 2013), showing its usefulness for a rapid flood risk assessment when spatial scale or the lack of detailed data make it impossible to use more sophisticated models. However, so far GFPLAIN has not been implemented for assessing large-scale flood exposure of large artificial landforms such as tailings deposits. The original GFPLAIN algorithm assumes that river floodplains associated with low-frequency events are naturally depicted in the terrain data (Nardi et al., 2006). The algorithm uses the 1D bivariate hydraulic equation proposed by Leopold and Maddock (1953) and Dodov and Foufoula-Georgiou (2004), described by Eq. (1) This equation corresponds to a scaling power law relation between the drainage area at a certain point within the river basin and its associated flood height associated with an extreme flood event.

$$FH = a \cdot Ad^{b} \quad (1)$$

https://doi.org/10.5194/egusphere-2022-122
Preprint. Discussion started: 11 April 2022

Eq. (1) is commonly known as the Hydraulic Scaling Relation (HSR), where FH represents the flow height in the river flood plain for a particular river cross section, in units of metres, *Ad* represents the drainage area of the river cross section [m^2], and *a* and *b* are empirical coefficients representing the geomorphic relationship between the hydraulics of the river section and the floodplain morphology. The *a* coefficient has units of [m^{-1}] and the *b* coefficient is dimensionless. Eq. (1) allows estimation of the water depth at peak flood flows along the stream network of the interest river basin. The coefficients of Eq. (1) are obtained fitting a power law distribution to (FH, Ad) observations as described in Section 2.5.

GFPLAIN uses Eq. (1), assuming a constant water level across a river transect, and available topographic data to determine the terrain cells that are inundated (Nardi et al., 2006; Nardi et al., 2013). The three input parameters required by GFPLAIN are an accumulation area threshold in units of km^2 (*bl_tresh*) and the values of *a* and *b* from Eq. (1). The value of *bl_tresh* represents the smallest drainage area to start delineating the stream network and its value is highly dependent on the input DEM and the river's morphology (McMaster, 2002). For this case study, the value was set fixed at 1 km^2 for all simulations to match the drainage density of Copiapó River Basin. This value was also found to minimize the number of floodplain widths smaller than 2 cells, in accordance with the recommendations made by Annis et al. (2019). The final output of GFPLAIN is a map showing flood extent and depth along the stream network and associated floodplains.

2.3 Model intercomparison

The results obtained with GFPLAIN were compared to results obtained with SWIFT in terms of its ability to predict the flood extent during extreme flood scenarios, and its ability to identify and prioritize tailings deposits exposed to these floods. This comparison was carried out for the modelling domain in which results were available for both models (see Fig. 1b) for two different flood scenarios; **1)** the observed flood event of March 2015 and **2)** a hypothetical flood event associated with a return period of 100 years. This comparison was carried out under the assumption of no infiltration losses. Infiltration can play an important role in 2D flood models (Huang et al., 2015), especially in arid regions (Ni et al., 2020; Tügel et al., 2020). However, this simplification was adopted for this SWIFT implementation to make the two modelling alternatives more comparable. GFPLAIN uses a hydrologically filled DEM as terrain input, which does not allow for ponding or accumulation of water on the surface and therefore overestimates the generation of runoff channels. Therefore, the runoff values obtained in the present study are likely to be overestimated or at best an approximation of locally generated runoff under the extreme scenario of saturated soil conditions.

Each modeling tool will be calibrated as described in Section 2.4 (SWIFT) and Section 2.5 (GFPLAIN), while Section 2.6 will present the methodology to evaluate the performance of GFPLAIN's results compared to SWIFT. Then, the flood maps obtained with each modelling alternative, for each flood event scenario, will be used to compare the exposure of tailings deposits as described in Section 2.7. Finally, a sensitivity analysis will be carried out as described in Section 2.8 to evaluate the changes in flood exposure of tailings deposits as a function of changes in the calibration of the HSR parameters used for GFPLAIN evaluation.

https://doi.org/10.5194/egusphere-2022-122
Preprint. Discussion started: 11 April 2022

2.4 Calibration and application of SWIFT

2.4.1 SWIFT calibration for the flood event of March 2015

SWIFT has been previously calibrated by Claro et al. (2018) using observed flood levels and mud heights surveyed by local authorities in the urban and peri-urban areas of Copiapó city and Tierra-Amarilla after the flood event of March 2015. The inflow hydrographs used by Claro et al. (2018) to model the flood event of 2015 are shown in Fig. 2a. The peak flows at Copiapó River and Quebrada Paipote during this event were estimated as 185 $m^3/$ sec] and 120 [m^3/sec], respectively. The rainfall time series used to model the event of 2015 corresponds to hourly measurements with a total cumulative precipitation depth of 22.7 mm over a period of 72-hour registered at the Copiapó city rain gauge (Fernández and Espinosa, 2020).

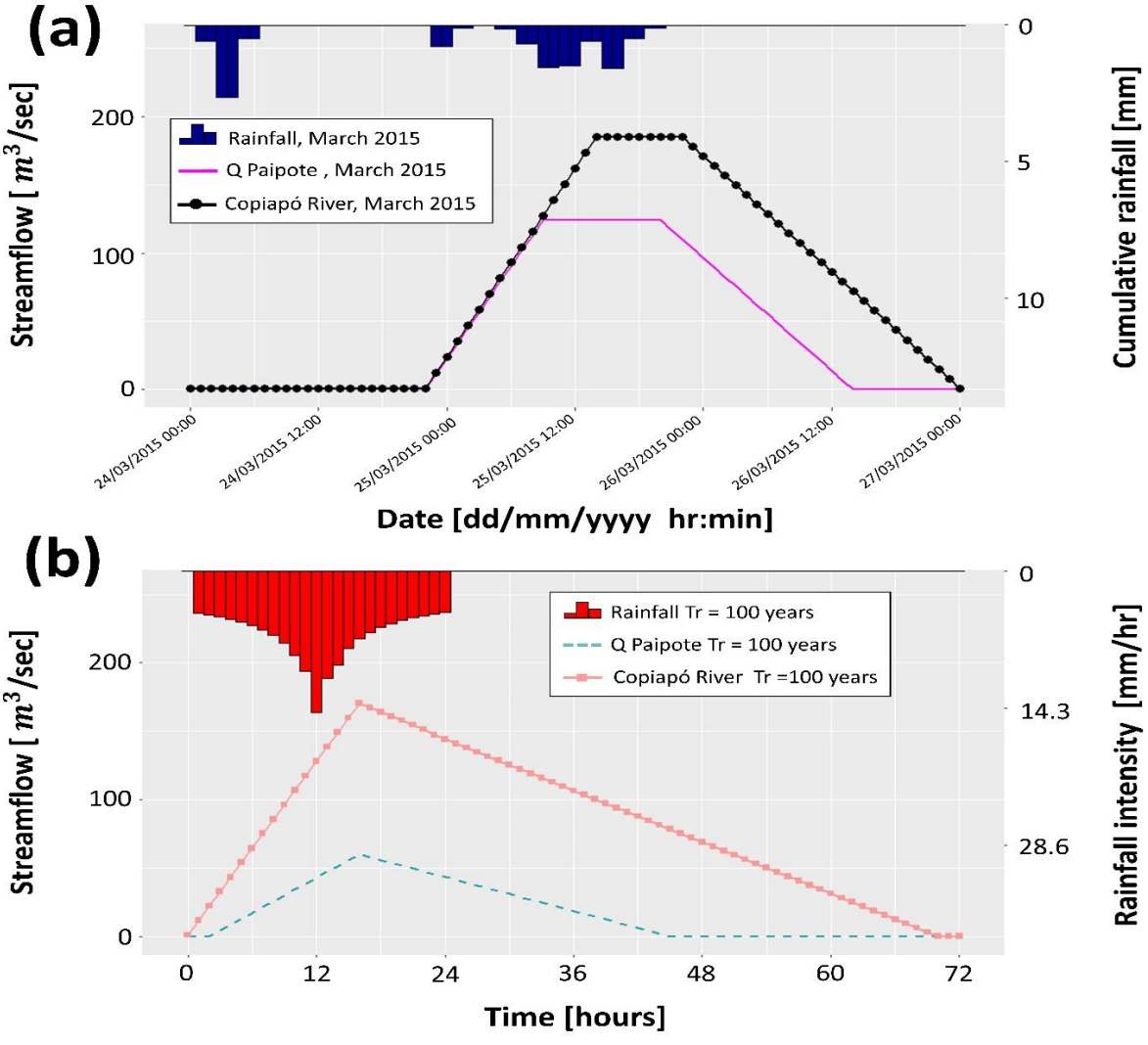

Figure 2. (a) Input hydrographs and rainfall time series (Copiapó city gauge) used to obtain SWIFT results for flood event of March 2015. **(b)** Synthetic triangular hydrographs and rainfall time series used to obtain SWIFT results for a return period of 100 years.

https://doi.org/10.5194/egusphere-2022-122
Preprint. Discussion started: 11 April 2022

The model was calibrated at a grid resolution of 5 m using Manning's roughness coefficient (*n*) values derived from a land use map published by Zhao et al. (2016) and the transformation from land use value to *n* proposed by Claro et al. (2018). The terrain data consisted of a mosaic of different moderate and high-resolution DTMs obtained from the Office for Hydraulic Works and the Ministry of Housing and Urbanism of Chile. Further information about input parameters and the model's configuration for the flood event of March 2015 can be found in Claro et al. (2018).

2.4.2 SWIFT's predictions for the flood event with a return period of 100 years

To be able to compare the results obtained with GFPLAIN for a return period (Tr) of 100 years, SWIFT was run using the flood hydrographs and a rainfall time series shown in Fig. 2b. The hydrographs for Copiapó River at Tierra-Amarilla and Quebrada Paipote at the entrance of Copiapó city were simplified as triangular synthetic hydrographs with time to peak equal to the concentration time (*Tc*) and the recession time (*Tf*) calculated using the unitless ratio of recession time to time to peak ($R_f = Tf/Tc$) (Granato, 2012). The value of R_f was estimated as 3.4 for Copiapó River and 2.1 for Quebrada Paipote based on analysis of historical streamflow records (DGA, 2021). The concentration times (*Tc*) for Copiapó river and Quebrada Paipote were calculated using the equations presented in Table 1.

Table 1. Equations for calculating concentration times

Parameter	Equation	Eq No
Concentration time (Tc)	$Tc = T_{co} + T_{cc}$,	(2)
Overland concentration time (Tco)	$Tco = 1.4394 \cdot \left(\frac{n_o \cdot L_o}{\sqrt{S_o}}\right)^{0.467}$,	(3)
Channel concentration time (Tcc)	$Tcc = \tau \cdot \left(\frac{0.87 \cdot CL}{1000 \cdot Sc}\right)^{0.385}$,	(4)

Tc is the conceptual concentration time [hours], $\mathbf{T_{co}}$ is overland concentration time and Tcc is the channel concentration time, $\mathbf{n_o}$ is the average Manning's coefficient of the drainage path, $\mathbf{L_o}$ is length of overland flow path [m], $\mathbf{S_o}$ the average overland slope [m/m], CL is the length of the longest water course [km], Sc is the average main watercourse slope [m/m], and $\boldsymbol{\tau}$ is a correction factor according to the accumulation area (Gericke and Smithers 2014). All the geomorphological variables were derived from the ALOS-Palsar RTC product (JAXA/METI-ASF, 2007), with a cell resolution of 12.5 m.

The peak streamflow values for Tr=100 years (Q_{100}) for the two river inflow points used by SWIFT (see Fig. 2b) are presented in Table 2. These values were calculated using Eq. (6) to make these results compatible with those obtained with GFPLAIN for the same return period (see Section 2.5.2).

Table 2. Parameters used to estimate synthetic hydrographs for Tr=100 years. Datum for inflows coordinates WGS 1984.

Inflow point	Longitude [Degrees]	Latitude [Degrees]	Tc [hr]	T_f [hr]	Q_{100} [m3/sec]
Q Paipote	70.26 ° E	27.39 ° S	14	29	60.1
Copiapó River	70.27 ° E	27.44 ° S	16	54	169.25

https://doi.org/10.5194/egusphere-2022-122
Preprint. Discussion started: 11 April 2022

The rainfall time series for Tr = 100 years was generated using the Intensity-Duration-Frequency relationships derived by Claro et al. (2018) for Copiapó city rain gauge for a 24-hour duration as described by Eq. (5).

$$I_{100} = 18.479 \cdot D^{-0.46} \quad (5)$$

Where I_{100} is the constant rainfall intensity [mm/hr] and D is rainfall duration [hours]. The rainfall time series was obtained using the alternate block method for a 24-hour duration following the methodology described by Chow et al. (1988). The rainfall time series used to run SWIFT for the Tr =100-year event is presented in Fig. 2b.

2.5 Calibration and application of terrain-based tool

The *a* and *b* parameters of Eq. (1) can be calibrated using values of flow height (*FH*) versus drainage area (*Ad*), representative of the Horton-Strahler orders of the river basin under study. For Copiapó River Basin the HSR parameters were estimated using 150 pairs of *FH* and *Ad* values, corresponding to 150 river cross-sections sampled randomly over its 5 streams orders. The estimation of *FH* values was made using a hydraulic analysis and a regional frequency analysis instead of the methodology based on the geomorphologic instantaneous unit hydrograph used by Nardi et al. (2006) and Nardi et al. (2013). The elevation profile of each river cross section was extracted from a high-resolution Digital Terrain Model (DTM) along the main Copiapó river and Quebrada Paipote channels (Claro et al., 2018) and from the ALOS-Palsar RTC product for the areas not covered by the DTM. The location of each river cross section and the 12.5 m DEM available for the entire river basin (JAXA/METI-ASF, 2007), were used to calculate the associated Ad value using the "D8" flow accumulation algorithm (Esri,2020). Then, the Ad values were used to estimate peak flows associated with a specific extreme flood event (see Section 2.5.1) or a specific return period (see Section 2.5.2). Once the streamflows were estimated for all the cross sections, *FH* values were calculated by means of a 1-D hydraulic analysis under the assumption of uniform flow. Finally, the pairs of *FH* and Ad values for each cross section were used to fit Eq. (1) and find the parameters *a* and *b*. The procedure used to obtain the HSR parameters is summarized in Fig. 3.

https://doi.org/10.5194/egusphere-2022-122
Preprint. Discussion started: 11 April 2022

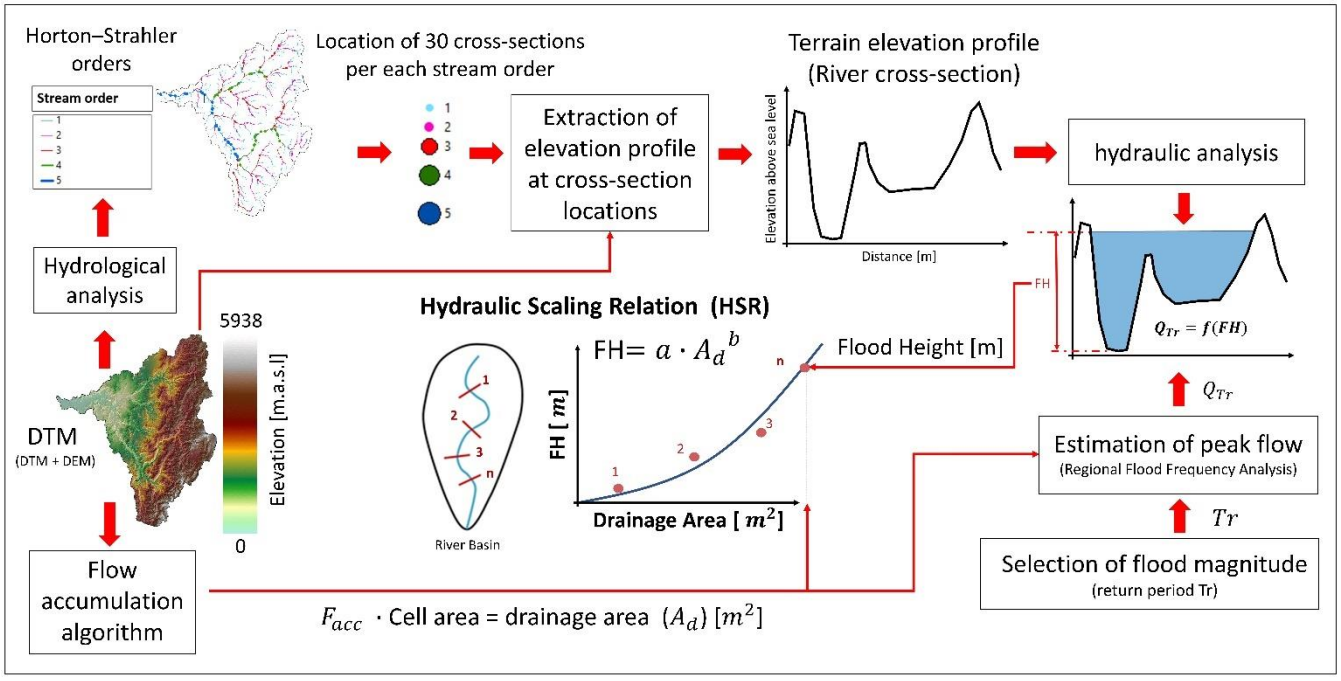

Figure 3. Schematic representation of the methodology used to obtain *a* and *b* coefficients of Hydraulic Scaling Relation (HSR) for Copiapó River Basin. This figure is a modification of the original version presented in Nardi et al (2013).

Annis et al. (2019) have provided an alternative approach to calibrate the HSR parameters, which uses pre-existing flood-hazard maps associated with low-frequency flood events (e.g., 100, 150, or 200 years return periods). However, such maps do not exist for Copiapó River Basin and do not exist in general for river basins of northern Chile. Therefore, the hydraulic analysis of river cross-sections described in this section was the only feasible option to calibrate the parameters of the HSR for Copiapó River Basin.

2.5.1 Calibration of HSR parameters for the flood event of March 2015

To obtain floodplain maps with GFPLAIN comparable to those of SWIFT for the event of March 2015, the streamflow values needed to calibrate the HSR parameters were estimated by scaling down the peak flows used for calibrating SWIFT (see Fig. 2a). This scale down procedure was carried all for all the river cross sections using Ad as the scale factor. These scaled down peak flows were used to obtain a set of *a* and *b* parameters as described in Fig. 3 and then the corresponding floodplain map using GFPLAIN.

2.5.2 Calibration of HSR parameters for a flood event with a return period of 100 years

To calibrate HSR for a return period of 100 years, the values of *FH* for each river cross section were obtained through a 1-D hydraulic analysis under uniform flow assumptions, solving Eq. (6) for *FH* to get a pair of (*FH, Ad*).

https://doi.org/10.5194/egusphere-2022-122
Preprint. Discussion started: 11 April 2022

$$Q_{Tr} = \frac{1}{n} \cdot A_w(FH) \cdot R(FH)^{1/3} \cdot S_o{}^{1/2} \quad (6)$$

Where Q_{Tr} represents the peak flow associated with a return period of *Tr* years $[m^3/sec]$, S_o is the local bed slope of the river channel [m/m], *R(FH)* is the hydraulic radius at the cross-section [m], which is a function of *FH*, $A_w(FH)$ is the cross-section area of flow $[m^2]$ as a function of *FH*, and *n* is the Manning's friction coefficient values. The *n* values for the case study region used in this research were taken from Claro et al., (2018). The average *n* values and drainage length per stream order are presented in Table 3, while the average value of *n* for the entire Copiapó river network was found to be 0.029.

Table 3. Average Manning's coefficient (n) for Copiapó River Basin drainage network

Strahler order	Number of streams	Drainage length [km]	Average *n*
1	327	1.8	0.020
2	69	850	0.036
3	15	525	0.028
4	3	228	0.026
5	1	184	0.035

Since the values of $A_w(FH)$ and $R(FH)$ can be expressed as a function of the river's flow height (*FH*), Eq. (6) can be solved explicitly for *FH* for any value of Q_{Tr}. The Q_{Tr} values for each cross section were calculated using the empirical relation described by Eq. (6), as proposed by the national Chilean handbook for extreme flow estimations (DGA, 1995).

$$Q_{Tr} = \frac{1}{3.6} \cdot C_{Tr} \cdot \ i_{t,Tr} \cdot A_d, \quad (7)$$

Where, C_{Tr} is an empirical loss coefficient associated with the river basin and the return period *Tr*, $i_{t,Tr}$ is the rainfall intensity [mm/hr] associated with the return period *Tr* and the catchment concentration time "t" in hours, and A_d is the drainage area in $[km^2]$.

2.6 Evaluation of model's performance

The ability of GFPLAIN to generate floodplain maps comparable to those obtained with SWIFT was evaluated using the metrics presented in Table 4. The Critical Success Index (CSI) and the False Alarm Ratio (FAR) were calculated based on a crossed error scheme, as proposed by Stephens et al., (2014); Sampson et al., (2015); and Wing et al., (2017), while the Root Mean Squared Error (RMSE) and the BIAS were calculated using the values of surface water elevation at 6 locations (see Fig. 5).

Table 4. Performance metrics used to assess performance of flood extent predictions.

Metric	Description	Equation	Eq No

https://doi.org/10.5194/egusphere-2022-122
Preprint. Discussion started: 11 April 2022

Critical Success Index (CSI)	The ability of GFPLAIN to reproduce the flood extent; ranges from 0 (poor) to 1 (perfect)	$$CSI = \frac{A}{A + B + C}$$	(8)
False Alarm Ratio (FAR)	The fraction of cells falsely modelled to be flooded by GFPLAIN; ranges from 0 (perfect) to 1 (poor)	$$FAR = \frac{B}{A + B}$$	(9)
Root Mean Squared Error (RMSE)	The magnitude of error in flood heights modelled by GFPLAIN	$$RMSE = \sqrt{\sum_{i=N}^{N} \frac{(WE_{SWIFT\,i} - WE_{GFPLAIN\,i})^2}{N}}$$	(10)
BIAS	Measures the overall bias of GFPLAIN: over prediction (positive) or under prediction (negative)	$$BIAS = \sum WE_{GFPLAIN\,i} - \sum WE_{SWIFT\,i}$$	(11)

A = Number of pixels correctly predicted as flooded by both models (hits); B = Number of pixels wrongly predicted as flooded by GFPLAIN; C = Number of pixels predicted as flooded by SWIFT but predicted as not flooded by GFPLAIN; D = Number of pixels correctly predicted as dry by both models; WE_{SWIFT} and $WE_{GFPLAIN}$ are the elevations of water surface for SWIFT' results and GFPLAIN's results respectively.

The performances of SWIFT and GFPLAIN against the flood observations made after the flood event of March 2015 were also evaluated using the metrics defined in Table 4, substituting observed flood observations into the equations where appropriate.

2.7. Evaluation of flood exposure of tailings deposits

The flood exposure of each tailings deposit was evaluated using the Flood Exposure Index (FEI) as defined in Eq. (12):

$$FEI = FPI \cdot FHRB\,, \tag{12}$$

Where, FEI is in units of [m], FPI corresponds to the Flood Proximity Index [-] and $FHRB$ corresponds to the flood height relative to the base of each deposit [m]. The FPI is defined as a binary variable (0/1) that indicates if the tailing's polygon intersects with flooded cells (FPI=1) or not (FPI=0). The values of $FHRB$ were calculated as the difference between the elevation at the base of each deposit and the maximum modelled surface water elevation in contact with the deposit.

2.8 Sensitivity analysis of Hydraulic Scaling Relation (HSR)

To explore the degree to which input assumptions may govern the performance of GFPLAIN, sensitivity analysis was conducted. The sensitivity of GFPLAIN's floodplain delineation and flood exposure results was evaluated through 22 modelling experiments grouped by three different factors: **1)** Friction coefficient (*n*), **2)** Sampled Stream Order (*SSO*), and **3)** Flow inputs. For each modelling experiment the HSR equation was fit to 100 sets of 150 river cross sections each. The final

https://doi.org/10.5194/egusphere-2022-122
Preprint. Discussion started: 11 April 2022

floodplain map for each modelling experiment was delineated using the *a* and *b* coefficients obtained after fitting Eq. (1) to all the (FH, Ac) points. The simulation chosen as the benchmark for the sensitivity analysis of the event of March 2015 was the HSR calibration using representative cross sections for all the Horton-Strahler orders (SSO= all), variable *n* coefficients according to the land use map as described in Section 2.5, and the scaled peak flows representative of the SWIFT calibration for the event of March 2015. The same sensitivity analysis was conducted for the results obtained for the hypothetical flood event with a return period of 100 years.

The sensitivity of the *a* and *b* parameters to *n*, was evaluated using four values of *n* (0.01, 0.02, 0.03, 0.05), that were kept uniform over all the sampled river cross sections. This range of *n* values was chosen to cover the estimated range of values in Table 3.

The sensitivities of the *a* and *b* parameters to *SSO* were evaluated by calibrating the HSR using four groups of Horton-Strahler orders: **a)** order 1 and 2; representative of runoff channels and ephemeral streams, **b)** order 2 and 3; representative of small streams, **c)** order 3 and 4; representative of permanent creeks and small streams, and **d)** order 4 and 5; representative of the main surface streams. The spatial resolution and the vertical accuracy of the terrain data used to calibrate HSR differs over the different Horton-Strahler orders. For stream orders 4 and 5, high-resolution DTMs with high levels of vertical accuracy were available, while for the rest of the river basin (stream orders 3 and lower), the only terrain data source available was the free 12.5 m pixel resolution ALOS-Palsar RTC product. Therefore, this experimental design will also provide some insights into the influence of terrain data quality on the calibration of HSR parameters.

Finally, to evaluate the influence of river inflows on the HSR parameters, the 1-D hydraulic analysis described in Fig. 3 was performed twice, **a)** estimating the peak flows at each river cross section by scaling the peak flows used for the calibrating SWIFT for the event of March 2015 (see Section 2.5.1) and **b)** estimating the peak flows for a return period of Tr = 100 years following the procedure described in Section 2.5.2.

3 Results

3.1 HSR calibration

Figure 4 presents the results of fitting Eq. (1) to the Flood Height (*FH*) and Drainage Area (*Ad*) data for the flood event of 2015, and the flood event with a return period of 100 years.

https://doi.org/10.5194/egusphere-2022-122
Preprint. Discussion started: 11 April 2022

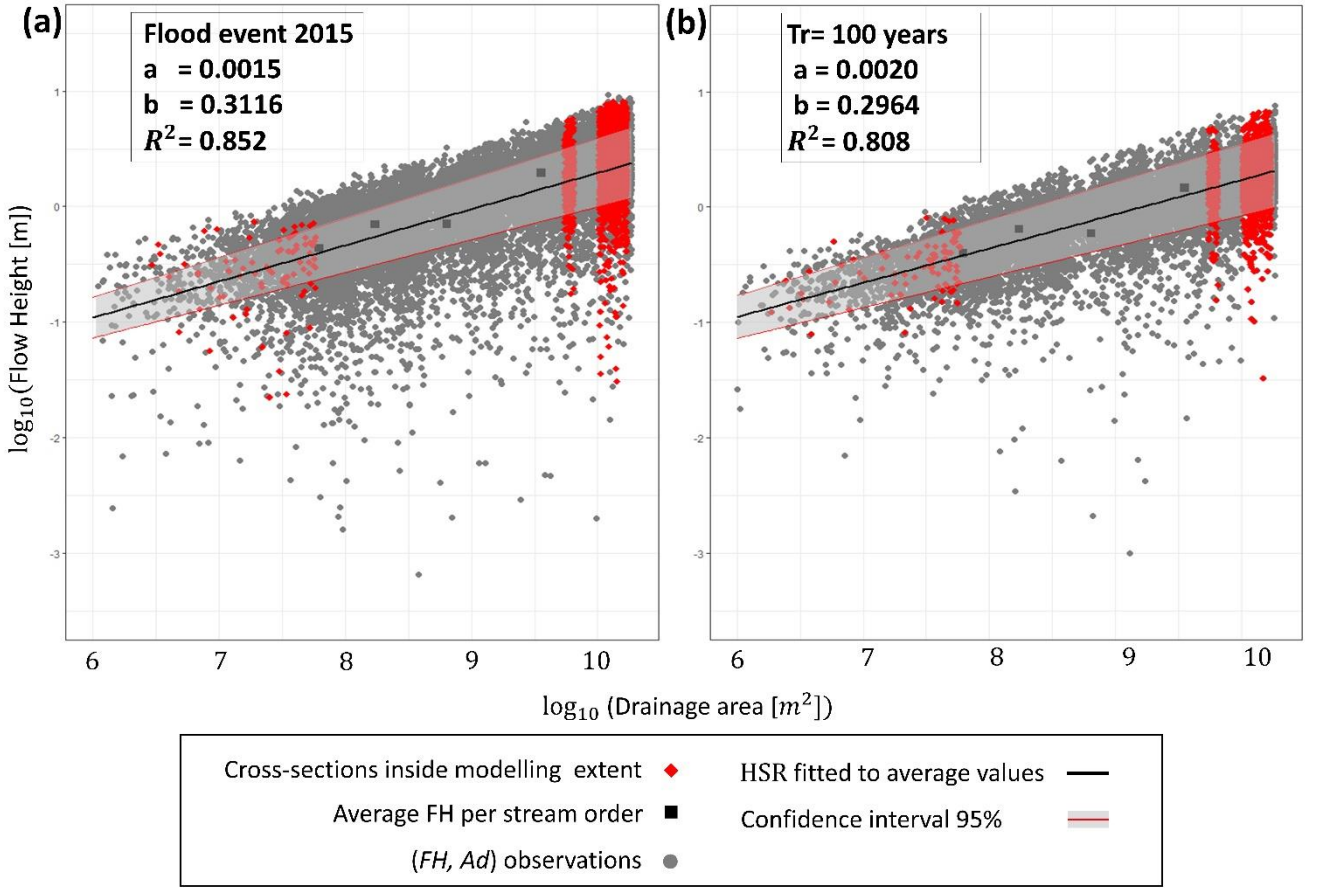

315 **Figure 4. (a)** HSR relation for Copiapó River Basin A: event of March 2015. **(b)** 100 years return period. Points within the model extent are plotted as red diamonds to indicate representativeness of the case study area in comparison to data from the entire river basin. The average FH values per stream order are presented as black squares.

Figure 4 shows that the data are explained by the power law models, $FH=0.0015Ad^{0.3116}$ in the case of the event of March 2015 and $FH=0.002Ad^{0.2964}$ for the flood event with a return period of 100 years. The uncertainty and adequacy of the HSR curves
320 fitted to these two flood scenarios will be discussed in more detail in Section 4.

3.2 Model intercomparison

3.2.1 Floodplain delineation

Figure 5 shows the floodplain extents obtained with SWIFT and GFPLAIN. The floodplain maps for the event of 2015 are plotted against the observed flood footprint obtained by the local authorities (red line on pink background). In general terms,
325 it can be observed that the flood maps obtained with GFPLAIN underestimate the flood extent obtained with SWIFT.

https://doi.org/10.5194/egusphere-2022-122
Preprint. Discussion started: 11 April 2022

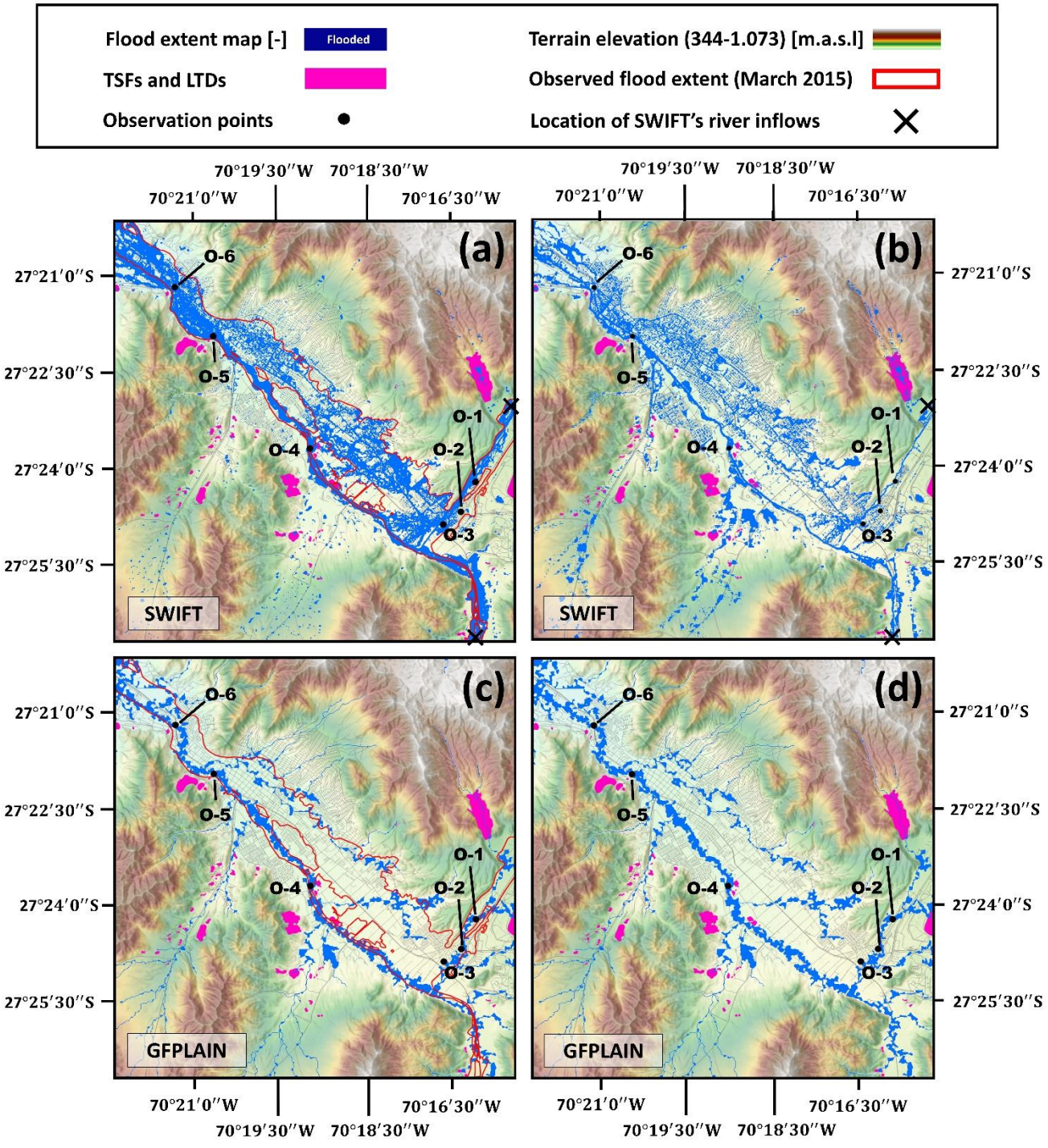

Figure 5. Flood extent maps for: **(a)** Flood event of March 2015 (SWIFT), **(b)** Return period of 100 years (SWIFT), **(c)** Flood event of March 2015 (GFPLAIN), **(d)** Return period of 100 years (GFPLAIN). The results obtained with SWIFT have a cell size of 5 m, while the results obtained with the modified version of GFPLAIN have a cell size of 12.5 m. All maps plotted with ALOS-Palsar RTC product (JAXA/METI-ASF, 2007) as background DEM.

https://doi.org/10.5194/egusphere-2022-122
Preprint. Discussion started: 11 April 2022

On the other hand, Fig. 6 presents the water depths at the observation points for these simulations.

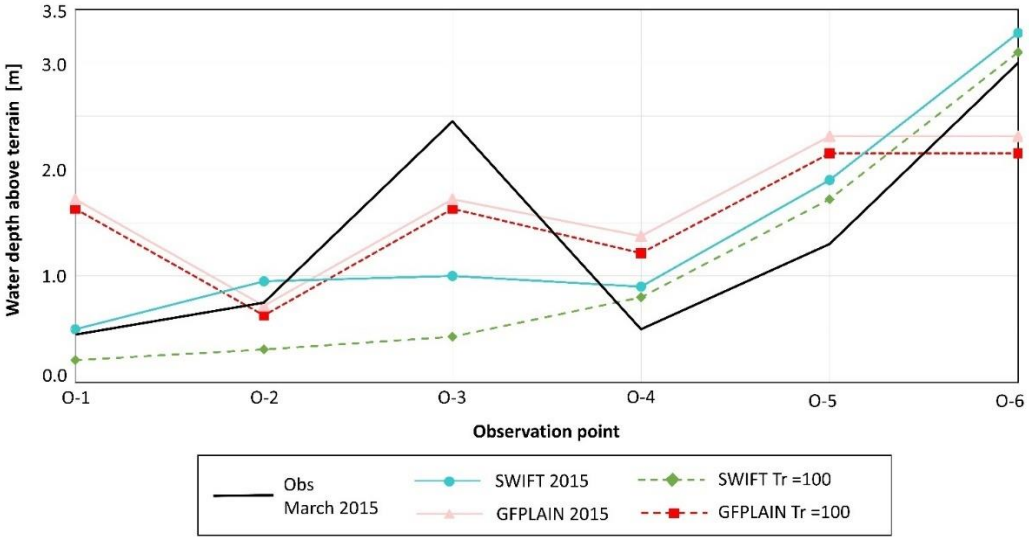

Figure 6. Water depth above terrain registered at observation points according to SWIFT and GFPLAIN.

Figure 6 shows there is little variation between the GFPLAIN results for the two flood scenarios, while the GFPLAIN's flood depths are higher than those obtained with SWIFT, except for points O-2 and O- 6. Considering that the peak flows used for calibrating the HSR are equivalent to the peak flows used as inputs to run SWIFT, these results suggest that GFPLAIN tends to over-estimate peak flow depths along the main river channels. These differences in flood heights are reflected in the performance of GFPLAIN's results when compared to SWIFT's results for the two flood scenarios summarised in Table 5. The reasons for and significance of the differences between GFPLAIN and SWIFT will be discussed in Section 4.1.

Table 5. Summary of GFPLAIN performance relative to SWIFT

Scenario	CSI	FAR	RMSE [m]	BIAS [m]
Event 2015	0.20	0.49	0.75	1.62
Tr = 100 years	0.17	0.60	0.90	2.83

3.2.2 Flood exposure of tailings deposits

The tailings deposits identified as exposed according to the two modelling alternatives and the two flood scenarios can be observed in Fig. 7. The FEI values for each tailings deposit and for each flood scenario are presented as columns in Table A1 of Appendix A.

https://doi.org/10.5194/egusphere-2022-122
Preprint. Discussion started: 11 April 2022

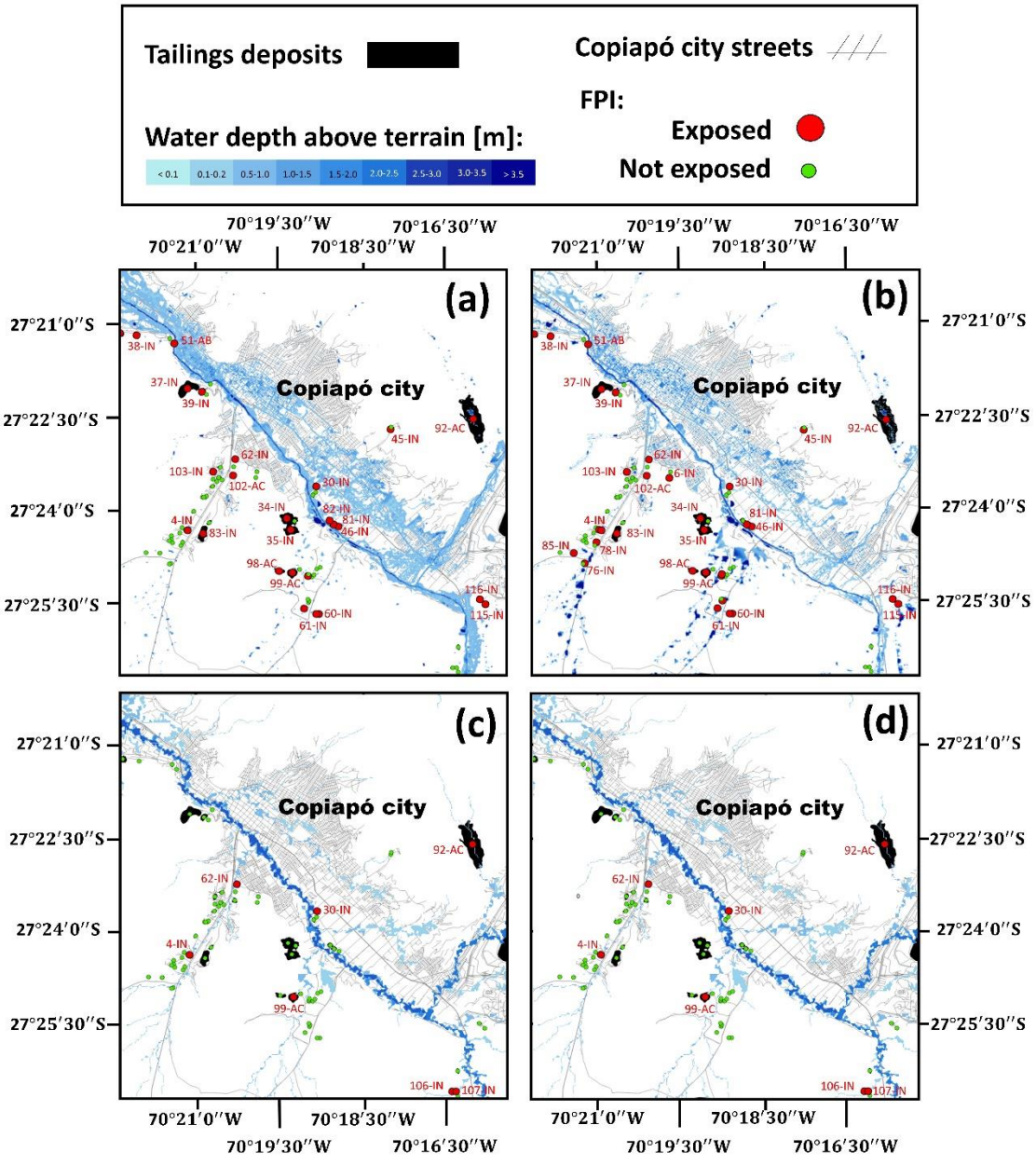

Figure 7. Flood proximity index of tailings deposits for different flood scenarios and two modelling alternatives. **(a)** SWIFT results for flood event of March 2015. **(b)** SWIFT results for flood event with Tr=100 years. **(c)** GFPLAIN results for flood event of March 2015. **(d)** GFPLAIN results for flood event with Tr=100 years.

Table 6 presents the flood exposure results and the top 10 deposits in terms of FEI values for each scenario presented in Fig. 7. The exposure results, for the 100-year return period, obtained with the floodplain map delineated by GFPLAIN for the entire Copiapó River basin are presented in Fig. C1 of Appendix C. The exposure map at a river basin scale for the event of March 2015 is not presented because it does not differ from the one obtained for a 100-year return period.

https://doi.org/10.5194/egusphere-2022-122
Preprint. Discussion started: 11 April 2022

Table 6. Prioritization of tailings deposits in terms of flood exposure index for 75 deposits inside the intercomparison extent.

Ranking	GFPLAIN March 2015		SWIFT March 2015		GFPLAIN Tr= 100		SWIFT Tr= 100	
	ID	FEI [m]	ID	FEI [m]	ID	FEI [m]	ID	FEI [m]
1	62-IN	0.35	92-AC	3.92	62-IN	0.36	92-AC	4.48
2	4-IN	0.33	99-AC	3.02	4-IN	0.34	28-IN	3.69
3	30-IN	0.31	51-AB	1.64	92-AC	0.21	99-AC	4.12
4	92-AC	0.20	80-AC	1.60	106-IN	0.17	80-AC	2.81
5	106-IN	0.16	39-IN	1.58	107-IN	0.17	39-IN	2.52
6	107-IN	0.16	42-IN	1.07	30-IN	0.15	29-IN	1.87
7	99-AC	0.13	33-IN	1.03	99-AC	0.13	4-IN	1.57
8	-	-	28-IN	0.98			42-IN	1.56
9	-	-	4-IN	0.97			33-IN	1.50
10	-	-	37-IN	0.73			98-AC	1.10
Total number of tailings deposits classified as exposed (FPI>0)	7		26		7		32	
Average FEI for exposed tailings deposits [m] (standard deviation)	0.22| (0.09)		0.83 (0.91)		0.23 (0.09)		1.05 (1.22)	

From Table 6, it can be observed that GFPLAIN only identifies as exposed 7 out of the 75 tailings deposits for both flood scenarios. The corresponding results for SWIFT suggest that 26 deposits were exposed to floodwaters during the event of March 2015, while 32 deposits are potentially exposed to flood waters under the flood scenario with Tr= 100 years. In addition to the relative underestimation of exposures by GFPLAIN, the standard deviation values in Table 6 show that degree of exposure (FEI) modelled by GFPLAIN varies relatively little among the deposits.

https://doi.org/10.5194/egusphere-2022-122
Preprint. Discussion started: 11 April 2022

Considering that the SWIFT simulation for the hypothetical 100-year event has a rainfall time series with significantly higher precipitation values but a smaller peak flow rate than those observed at Copiapó during the 2015 event, it is possible to conclude that the larger number of tailings deposits identified as exposed in the former event is due to locally generated rainfall rather than overflow of Copiapó River or Quebrada Paipote. On the other hand, it can be observed that the flood height values of deposits directly exposed by the overflow of the Copiapó River were lower for the 100-year return period scenario, since the peak flows used to model this event were smaller than those used to represent the event of March 2015. For example, the height of the flood waters above the base of deposit 51-AB decreased from approximately 1.64 m under the 2015 event to 0.85 m under the 100-year event (see Table). Moreover, a similar reduction in FEI values was observed for deposits 30-IN, 46-IN and 81-IN, all of which were considered exposed due to the overflow of the Copiapó River. Therefore, interpreting exposures and differences in results between events and models must consider the flooding mechanisms.

Deposits 92AC, 99-AC and 4-IN are consistently identified amongst the highest priority in terms of flood exposure by both modelling alternatives and for the two evaluated flood scenarios. On the contrary, the deposit 107-IN was the only deposit identified as exposed by the GFPLAIN that was not identified as exposed by SWIFT for either of the two flood scenarios. These results will be further discussed in the Section 4.3.

3.3 Sensitivity analysis

The sensitivity of the *a* and *b* coefficients to changes in *n* and to the SSO for a return period of 100 years are summarized in Table 7. This table shows that the values of *a* and *b* increase as *n* increases, suggesting an increase in the resulting floodplain extent and predicted flood height magnitudes. Additionally, it can be observed that the values of *b* increase and the values of *a* decrease as SSO increases. Since the effect of *b* coefficient on the flow height values is exponential, the overall effect of selectively fitting the HSR to river cross sections associated with higher stream orders is an increase in the floodplain extent and the resulting flood depths.

https://doi.org/10.5194/egusphere-2022-122
Preprint. Discussion started: 11 April 2022

Table 7. Sensitivity of HSR parameters to Manning's coefficient (n) and Sampled Stream Order (SSO) for a return period of 100 years.

n	Sensitivity to Manning's coefficient (n)		SSO	Sensitivity to Sampled Stream order (SSO)	
	a (SD[1])	b (SD[1])		a (SD[1])	b (SD[1])
According to map (average =0.029)	0.002 (0.0003)	0.296 (0.017)	**All**	0.002 (0.0003)	0.296 (0.017)
0.01	0.0011 (0.0002)	0.314 (0.021)	**1 and 2**	0.0043 (0.0005)	0.166 (0.01)
0.02	0.0018 (0.0003)	0.300 (0.018)	**2 and 3**	0.0029 (0.0004)	0.262 (0.011)
0.03	0.0021 (0.0003)	0.298 (0.018)	**3 and 4**	0.0023 (0.0003)	0.284 (0.013)
0.05	0.0024 (0.0003)	0.300 (0.018)	**4 and 5**	0.0018 (0.0003)	0.303 .019)

[1]SD= standard deviation of the estimate

Despite the sensitivity of *a* and *b* to the HSR model inputs seen in Table 7, this had very little effect on the flood exposure of tailings deposits and on the CSI, FAR, RMSE and BIAS metrics used to compare the GFPLAIN and SWIFT results (see Fig. B1 of Appendix B). This implies that GFPLAIN may result in important errors that are not related to the HSR model inputs, as discussed later. Figure 8 shows variation between the deposits identified as exposed by each sensitivity scenario and those exposed under the benchmark GFPLAIN run for the 100-year event. Sensitivities are shown for both the Copiapó city region (Fig. 8a) and for the entire river basin (Fig. 8b). The variation in the number of exposed deposits is moderate at both and river basin scales but the variation in the priority (most exposed) deposits is higher. For example, when considering the entire river basin, changing from the benchmark value of *n* to *n* = 0.05 leads to 70% of the priority deposits changing. The corresponding results for the March 2015 event were similar.

https://doi.org/10.5194/egusphere-2022-122
Preprint. Discussion started: 11 April 2022

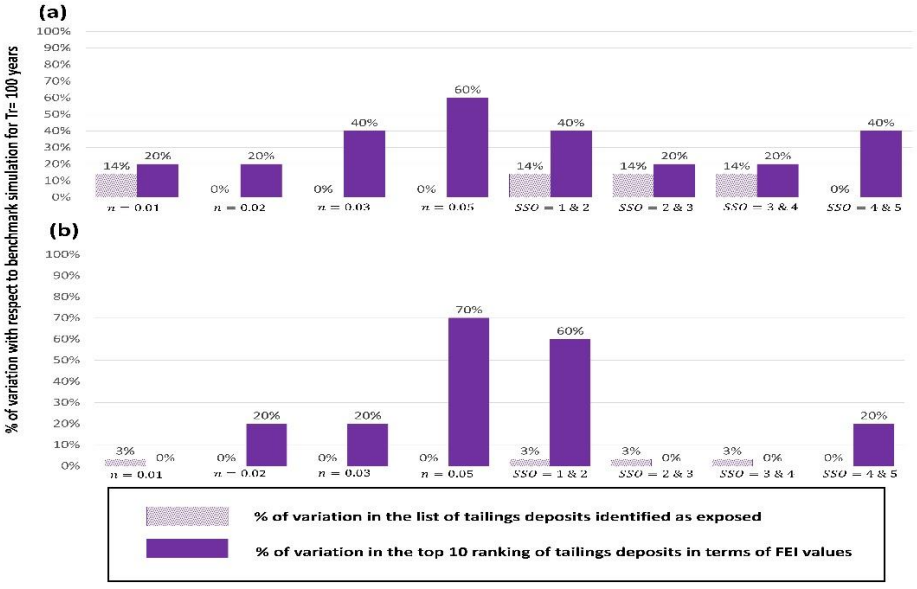

Figure 8. Sensitivity of flood exposure and prioritization of tailings deposits to changes in Manning's coefficients (n) and Sampled Stream Order (SSO) for floodplain predictions associated with a return period of 100 years. **(a)** Percentage of variation in exposure results for 75 deposits inside the intercomparison region (Copiapó city and surroundings). **(b)** Percentage of variation in exposure results for the entire Copiapó River Basin (118 deposits).

4. Discussion

4.1 Comparison of floodplain delineations obtained with GFPLAIN and SWIFT

In general terms, the floodplain delineation obtained with GFPLAIN near the main river channels can be considered a good approximation of the results obtained with the hydrodynamic model. However, the flood delineation obtained with GFPLAIN in the wider floodplains of Copiapó city region is not a good approximation of the delineation obtained with SWIFT. The differences cannot be attributed to the magnitudes of the peak flows used for calibrating the HSR parameters since both models were run using equivalent peak flows. Instead, the differences may be attributed to limitations of GFPLAIN's simplifications of the flow dynamics and exogenous factors such as the low vertical accuracy of the available terrain models used to calibrate GFPLAIN. The one-dimensional uniform flow assumptions behind Eq. (6) become invalid in river reaches in which transitions from high to low slope occur, making backwater effects more relevant. As can be observed in Fig. 5, some regions of the modelling domain can be classified within this slope transition zone. Additionally, the anthropogenic terrain modifications in Copiapó also limit the applicability of Eq. (1) and the accuracy of the subsequent GIS-based floodplain delineation process. Moreover, the ALOS-Pulsar RTC product used to delineate the floodplain maps and to extract the river cross-section elevation profiles for streams with Strahler order 3 or lower limits the accuracy of GFPLAIN's calibration and delineation processes, especially in urbanized regions. Where terrain data of higher vertical accuracy are available, GFPLAIN can be expected to obtain better results (e.g Nardi et al., 2006; Nardi et al., 2013 and Annis et al., 2019).

https://doi.org/10.5194/egusphere-2022-122
Preprint. Discussion started: 11 April 2022

Another accuracy consideration is that the flood levels obtained with both models for the event of March 2015 slightly overestimate the surveyed flood levels (see Fig. 6). This overestimation could have been caused by many factors including the underestimation of infiltration losses and the uncertainty associated with the estimation of flow inputs. Therefore, it is recommended to evaluate the influence of these factors in future flood modelling attempts of the Lower Copiapó River Basin at the modelled area.

4.2 Sensitivity of HSR coefficients and exposures

Based on the results presented in Section 3.3, it was possible to conclude that neither the accuracy of GFPLAIN relative to SWIFT nor the total number of tailings deposits identified as exposed by GFPLAIN are highly sensitive to the evaluated range of Manning's coefficient (*n*). However, the results showed in Fig. 8 revealed that *n* does affect the prioritization of deposits. Nevertheless, these changes do not affect the general performance of the GFPLAIN when compared to SWIFT. The sensitivity analysis also showed that the prioritization was sensitive to the stream order (*SSO*) of the river cross-sections used to calibrate the HSR parameters of GFPLAIN. The most noticeable changes (Fig. 8) were obtained when the HSR was calibrated using only the lower order channels, *SSO* =1 and *SSO* =2, followed by the results obtained using cross sections along the main river channels, *SSO* = 4 and 5. It is concluded that using GFPLAIN with HSR parameters calibrated with river cross-sections that are not sufficiently representative of the entire river basin can have a significant effect on the prioritization of deposits. Finally, Fig. 4 showed that reducing the magnitude of the flow rates used to calibrate HSR reduces GFPLAIN's flood height predictions, while Fig. 5 and Table 6 showed that the effects of this on the modelled floodplain extent are minor. The list of exposed deposits obtained for the flood scenario of March 2015 is the same as the list obtained for a return period of 100 years with differences only in the order of priority (see Table 6). These results suggest that the magnitude of the peak flows used to calibrate the HSR parameters was not the most relevant factor affecting the prioritization obtained with GFPLAIN in this study.

4.3 Flood exposure of tailings deposits in Copiapó River Basin

Based on the exposure maps presented in Fig. 7 and results in Table 6, it can be observed that the total number of tailings deposits identified as exposed when using GFPLAIN is lower than when using SWIFT for both flood scenarios. For both flood scenarios, GFPLAIN identified only 5 of the deposits that SWIFT identified to be exposed (4-IN, 30-IN, 62-IN, 92-AC, and 99-AC). These results allow us to conclude that GFPLAIN has significant limitations in providing an accurate and complete prioritization of tailings deposits exposed to floods in the urban and peri-urban area of Copiapó city, where the comparison was made. Since a major source of error in GFPLAIN is the generalised hydraulic equation and low resolution of the DEM, it is likely that the same limitations apply to the whole basin.

Most of the tailings deposits identified as exposed in this case study region are inactive. For example, for the 2015 event, 17 out of 31 identified as exposed by GFPLAIN at a river basin scale and 20 out of 26 identified as exposed by SWIFT in the intercomparison region are classified as inactive.

https://doi.org/10.5194/egusphere-2022-122
Preprint. Discussion started: 11 April 2022

Analysing the location of some of the deposits can provide further insight into the potential flood exposure mechanisms. 4-IN, identified as exposed by both models (see Table 6), is located more than 500 m away from Copiapó River and any of its main tributaries, but close to the embankment of a main road. This suggests its exposure may be due to runoff accumulation along terrain depressions that align with this road. On the contrary, deposit 30-IN is located less than 200 m from the right bank of Copiapó river and approximately 3 m above the river's bed. According to the flood maps obtained with SWIFT and GFPLAIN, this deposit was exposed to water overflowing from Copiapó River. On the other hand, the location, and characteristics of deposit 106-IN (see lower right corner of Fig.7c and Fig.7d), modelled to be exposed by GFPLAIN, is located approximately 10 m above the Copiapó riverbed, suggesting that if it was exposed to floodwaters during the flood event of March 2015, it was due to its location near an ephemeral runoff channel rather than the overflow of Copiapó River. A possible explanation as to why 106-IN was not identified as exposed by SWIFT could be because the terrain data used in GFPLAIN has lower spatial resolution and poorer vertical accuracy, which may smooth the terrain features and exaggerate or distort some of the runoff channels. Nevertheless, this example is representative of the GFPLAIN basin-scale results, indicating the potential importance of the relatively small ephemeral tributaries.

It is noteworthy that deposit 51-AB was not identified as exposed by GFPLAIN in either of the flood scenarios, despite being less than 50 m away from the left bank of Copiapó River. According to the GFPLAIN results for the 2015 event, the maximum flood depth at the river cross-section closest to deposit 51-AB was 2.31 meters, which is significantly lower than the 4.4 m modelled by SWIFT at the same location. This location offers a clear example of the limitations of GFPLAIN to adequately represent the hydraulics of the river channel in floodplain areas with relatively low slopes.

Finally, it is important to note that the flood exposure results presented in this research are only indicative of the potential flood hazard derived from the deposits' locations within the floodplain. The actual flood hazard of individual tailings deposits depends on the physical and geochemical characteristics of each deposit, and the existing infrastructure design to divert and collect runoff and seepage. Additionally, other aspects of the flood's dynamics such as flood velocity and inundation times are essential to determine the amounts of tailings that can be potentially eroded from each site.

4.4 Applicability of terrain-based flood mapping tool for assessing flood exposure of tailings deposits

Since terrain-based flood mapping tools are unable to quantify essential aspects of the flood dynamics (e.g. flow velocities and flood times), these tools only identify the stretches of river where a hydrodynamic model is needed to better understand erosion potential. For example, the floodplain maps delineated by the GFPLAIN identified the section immediately upstream of Quebrada Carrizalillos, at the confluence of this creek with Copiapó River, as target for further exposure assessment for deposits 43-AC and 44-AC. Similarly, the prioritization obtained with GFPLAIN suggest that it is important to make a more detailed evaluation of the fluvial dynamics of Copiapó River in the section between the mouth of Quebrada Carrizalillos and the town of San Antonio, located 25 km upstream from deposit 47-AB.

Regarding the moderate sensitivity of GFPLAIN results to some hydraulic model inputs (*n* and *SSO*) it is important to recognise that this tool focuses on the floodplain geomorphology as the main predictor of the flood extent and height, with limited regard

https://doi.org/10.5194/egusphere-2022-122
Preprint. Discussion started: 11 April 2022

to other factors affecting local hydraulics. This tool is expected to be a reasonably good approach where flow conditions are near to a typical normal depth, and the underlying assumptions of the HSR are valid. The case study area showed GFPLAIN's limitations for more hydraulically complex situations, where depths are affected by urban features such as bridges, buildings, and anthropogenic terrain modifications. Additionally, as can be observed in Fig. 4, the HSR model smooths out the high variability between the flood depths at different sections of the river system, even for the drainage areas representative of the study area (red dots), illustrating the uncertainty associated with the use of the GFPLAIN in this case study. Partly for these reasons, GFPLAIN showed significant limitations in reproducing the results obtained with SWIFT.

GFPLAIN's limitations to correctly reproduce SWIFT's results could also be attributed to the use of a moderate resolution satellite-derived DEM (ALOS PALSAR RTC product) to supplement the areas where the high-resolution DTM was not available. Therefore, it is worth evaluating the applicability of GFPLAIN for the purposes explored in this research, in other remote regions around the world where Digital Surface Models (DSMs) with better vertical and horizontal accuracies are available.

Finally, the results obtained in the intercomparison region indicate that the modified version of GFPLAIN used in this study should not substitute a hydrodynamic model for mapping the extent of low frequency floods (see Fig. 7) or the prioritization of tailings deposits potentially exposed to floods (see Table 6) . However, the prioritization results showed in Table 6 suggest that the evaluated terrain-based tool can potentially identify some of the flooded deposits that should be prioritized (e.g. 4-IN, 30- IN,92AC and 99-AC). Therefore, terrain-based tools, such as GFPLAIN, can be considered valuable for a first assessment of flood exposure of tailings located within river floodplains. Considering this, the results obtained with this modified version GFPLAIN, far from replacing results obtained with a 2D hydrodynamic models like SWIFT, may be treated as a first approach to the delineation of flood maps, especially in remote areas under sparse data conditions.

5 Conclusions

This research has provided evidence of the potential flood exposure of at least 28 tailings storage facilities and 3 legacy tailings deposits inside Copiapó River Basin. These results, although limited by the modelling assumptions, are the first step towards a comprehensive flood hazard assessment of tailings deposits in northern Chile. The model intercomparison has improved understanding of the limitations of terrain-based floodplain delineation tools such as GFPLAIN and their applicability for estimating flood hazard in the absence of national fluvial flood maps. A principal limitation in the applicability of the modified version of GFPLAIN tested in this research was the use of freely available DEMs with low vertical accuracy. Thus, it is recommended to carry out additional evaluations of GFPLAIN or comparable algorithms in other basins, where it is possible to calibrate the HSR parameters, either with pre-existing flood maps or flood observations or with high-resolution terrain data.

https://doi.org/10.5194/egusphere-2022-122
Preprint. Discussion started: 11 April 2022

6. Appendices

Appendix A. List of tailings deposits inside Copiapó River Basin

Table A1. List of tailings deposits inside Copiapó River Basin and values of Flood Exposure Index (FEI) according to the flood maps obtained with each modelling alternative for each flood scenario (Event of March 2015 and Tr= 100 years). Tailings deposit's information provided by the Chilean Service of Geology and Mining (SERNAGEOMIN, 2020). Coordinates correspond to the centroid of each tailing's polygon given in CRS: SIRGAS-Chile UTM Zone 19S, Transverse Mercator

ID	E coordinates [m]	N coordinates [m]	Type	Commodity	Deposit's name	Owner	FEI [m] GFPLAIN 2015	FEI [m] SWIFT 2015	FEI [m] GFPLAIN Tr 100 years	FEI [m] SWIFT Tr 100 years
1-AC	366309.267	6968008.71	Dam	Cu	embalse de relaves	Acibol spa	0	0	0	0
2-IN	366009.522	6967767.067	Dam	Au-Cu	embalse de relave	Ana Maria Munizaga	0	0	0	0
3-IN	366409.177	6967950.376	Dam	Cu-Au	florencia 2	Carlos Iribarren	0	0	0	0.41
4-IN	366477.463	6967927.743	Dam	Cu-Au	florencia 1	Carlos iribarren	0.33	0.97	0.34	1.57
5-IN	368496.231	6969678.012	Tailings embankment	Cu	porvenir	Carlos soto fuentealba	0	0	0	0
6-IN	368453.271	6969503.293	Tailings embankment	Cu	porvenir sur	Carlos soto fuentealba	0	0	0	0.42
7-AC	370496.720	6956876.851	Tailings embankment	Cu	Candelaria	CIA. contractual minera Candelaria	0.21	-	0.22	-
8-IN	372241.969	6959137.25	Tailings embankment	Cu	san esteban 1 principal	CIA. contractual minera Candelaria	0.17	-	0.18	-
9-IN	372145.672	6958753.084	Tailings embankment	Cu	san esteban 2	CIA. contractual minera Candelaria	0.17	-	0.18	-
10-IN	372548.932	6959207.422	Tailings embankment	Cu	san esteban 1 secundario	CIA. contractual minera Candelaria	0.18	-	0.19	-
11-IN	369845.261	6953631.957	Tailings embankment	Cu	los diques	CIA. contractual minera Candelaria	0.25	-	0.26	-
12-IN	382835.295	6933622.032	Tailings embankment	Cu	elisa de bordos 2	CIA. exploracion de minas San Andres	0	-	0	-
13-IN	382777.612	6933374.327	Tailings embankment	Cu	elisa de bordos 1	CIA. exploracion de minas San Andres	0.15	-	0.16	-
14-AC	382854.453	6932952.615	Tailings embankment	Cu	elisa de bordos 3	CIA. exploracion de minas San Andres	0.17	-	0.18	-

https://doi.org/10.5194/egusphere-2022-122
Preprint. Discussion started: 11 April 2022

15-IN	383071.170	6933484.67	Tailings embankment	Cu	tranque de relave	CIA. exploracion de minas San Andres	0.15	-	0.16	-
16-IN	471285.637	6984758.391	Tailings embankment	Cu	la pepa 1	CIA. minera horus	0	-	0	-
17-IN	471331.991	6984868.463	Tailings embankment	Cu	la pepa 2	CIA. minera horus	0	-	0	-
18-IN	472011.55	7032410.376	Filtered_tailings	Au-Cu	rahco	CIA. minera mantos de oro	0.2	-	0.21	-
19-IN	472729.824	7033092.551	Filtered_tailings	Au-Cu	rahco	CIA. minera mantos de oro	0	-	0	-
22-IN	375598.469	6958029.923	Tailings embankment	Cu-Au	pedro aguirre cerda 1	CIA. minera ojos del salado	0	-	0	-
24-IN	375454.938	6957984.333	Tailings embankment	Cu-Au	pedro aguirre cerda 2	CIA. minera ojos del salado	0	-	0	-
23-IN	375532.545	6957868.573	Tailings embankment	Cu-Au	pedro aguirre cerda 3	CIA. minera ojos del salado	0.11	-	0.12	-
20-IN	375314.048	6958569.142	Tailings embankment	Cu-Au	pedro aguirre cerda 4-6	CIA. minera ojos del salado	0	-	0	-
21-IN	375394.936	6958142.891	Tailings embankment	Cu-Au	pedro aguirre cerda 5	CIA. minera ojos del salado	0	-	0	-
25-IN	365271.131	6967269.73	Tailings embankment	Au	amanda (ex charito)	CIA. minera oro verde	0	0	0	0
26-IN	370090.958	6966545.66	Dam	Au	embalse de relaves	CIA. minera purificacion	0	0	0	0
27-IN	369985.367	6966535.614	Tailings embankment	Au	purificacion 1	CIA. minera purificacion	0	0	0	0
28-IN	369984.264	6966579.661	Tailings embankment	Au	purificacion 2	CIA. minera purificacion	0	0.98	0	3.69
29-IN	369992.450	6966626.383	Tailings embankment	Au	purificacion 3	CIA. minera purificacion	0	0	0	1.87
32-IN	370214.072	6969242.793	Tailings embankment	Cu	san esteban 1	CIA. minera San Esteban	0.31	0.36	0.15	0.22
30-IN	370197.660	6969057.295	Tailings embankment	Cu	san esteban 2a	CIA. minera San Esteban	0	0	0	0
31-IN	370130.858	6968978.424	Tailings embankment	Cu	san esteban 2b	CIA. minera San Esteban	0	0	0	0
34-IN	369482.2977	6967939.028	Tailings embankment	Cu	santa laura 1	CIA. minera San Esteban primera	0	1.03	0	1.5
33-IN	369367.4046	6968289.618	Tailings embankment	Cu	santa laura 2	CIA. minera San Esteban primera	0	0.64	0	0.65
35-IN	369583.8416	6968202.972	Tailings embankment	Cu	santa laura 3	CIA. minera San Esteban primera	0	0	0	0
36-IN	367218.1591	6969451.221	Tailings embankment	Cu	tranque de relave	CIA. minera San patricio	0	0	0	0
37-IN	366467.7245	6972143.373	Tailings embankment	Cu	ojancos 2	cmc sali hochschild S.A	0	0.73	0	0.14
38-IN	364994.0624	6973725.94	Tailings embankment	Cu-Au	deposito de relave 3	cmc sali hochschild S.A	0	0.34	0	0.86
39-IN	366892.5618	6972053.496	Tailings embankment	Cu	ojancos 1	cmc sali hochschild S.A	0	1.58	0	2.52
40-IN	364291.1512	6973740.38	Tailings embankment	Cu-Au	deposito de relave 4	cmc sali hochschild S.A	0.24	-	0.25	-
41-IN	367131.3649	6972271.062	Tailings embankment	Cu	tranque de relave	cmc sali hochschild S.A	0	0	0	0

https://doi.org/10.5194/egusphere-2022-122
Preprint. Discussion started: 11 April 2022

42-IN	364511.3082	6973783.277	Tailings embankment	Cu-Au	bodega alto	cmc sali hochschild S.A	0	1.07	0	1.56
43-AC	378304.2912	6949531.401	Tailings embankment	Cu	tranque de relave 3	COEMIN S.A	0.98	-	0.95	-
44-AC	377274.2513	6950496.535	Tailings embankment	Cu	tranque de relave 1	COEMIN S.A	0.2	-	0.21	-
45-IN	372382.1541	6970934.887	Dam	Au-Cu	andrea	comercial Ledesma representaciones	0	0.23	0	0.21
46-IN	370868.9665	6968039.105	Tailings embankment	Cu-Au	tania	Delia Nieto Roble	0	0.20	0	0.16
47-AB	378091.8825	6940569.173	Tailings embankment	Cu	pabellon	Unknown	1.88	-	1.77	-
48-IN	370159.3128	6966609.624	Tailings embankment	Au	tranque de relave	Unknown	0	0	0	0
49-IN	370240.0586	6966791.892	Tailings embankment	Au	tranque de relave	Unknown	0	0	0	0
50-IN	370325.4351	6966830.753	Tailings embankment	Au	tranque de relave	Unknown	0	0	0	0
51-AB	366095.4674	6973477.761	Tailings embankment	Cu	tranque de relave	Unknown	0	1.64	0	0.85
52-AB	365965.53	6973625.619	Tailings embankment	Au-Cu	guggiana	Domingo guggiana	0	0	0	0
53-IN	366907.5838	6968914.74	Tailings embankment	Au	santa teresa 1	Elias resk contreras (soc. minera Santa teresa)	0	0	0	0
54-IN	366983.4519	6968911.606	Tailings embankment	Au	santa teresa 3	Elias resk contreras (soc. minera Santa teresa)	0	0	0	0
55-IN	367019.044	6968940.171	Tailings embankment	Au	santa teresa 4	Elias resk contreras (soc. minera Santa teresa)	0	0	0	0
56-IN	366949.3712	6968922.724	Tailings embankment	Au	santa teresa 2	Elias resk contreras (soc. minera Santa teresa)	0	0	0	0
57-AC	376075.261	6968309.231	Tailings embankment	Cu	tranque de relave 3	ENAMI	1.72	-	1.63	-
58-IN	376394.5134	6967600.241	Tailings embankment	Cu	tranque de relave 1	ENAMI	0	-	0	-
59-IN	376013.4333	6967361.995	Tailings embankment	Cu	tranque de relave 2	ENAMI	0	-	0	-
60-IN	370300.7407	6965446.19	Dam	Au	santa rosa 2	exequiel bugueño	0	0.46	0	0.16
61-IN	370212.297	6965436.563	Dam	Au	santa rosa 1	exequiel bugueño	0	0.26	0	0.32
62-IN	367857.955	6970045.911	Tailings embankment	Au	castellon	Hector castellon	0.35	0.20	0.36	0.3
63-AC	398249.479	6894600.647	Dam	Cu	embalse de relaves	inversiones e inmobilaria copayapu	0.22	-	0.23	-
64-IN	370318.903	6962897.734	Tailings embankment	Cu	desconocido	inversiones ray ltda.	0	-	0	-

https://doi.org/10.5194/egusphere-2022-122
Preprint. Discussion started: 11 April 2022

65-IN	370262.954	6962952.183	Tailings embankment	Cu	desconocido	inversiones ray ltda.	0	-	0	-
66-IN	367020.916	6971972.925	Tailings embankment	Cu	desconocido	Luis morales	0	0	0	0
67-AB	337536.015	6967571.821	Tailings embankment	Cu	tranque de relave	Luis padilla	0	-	0	-
68-IN	367815.389	6969820.183	Tailings embankment	Cu-Au	cuesta cardones 1	manuel achu perez	0	0	0	0
69-IN	362855.091	6966457.62	Dam	Cu	embalse maya	maya enterprises ltda.	0.17	-	0.18	-
70-AC	367384.250	6969499.406	Tailings embankment	Au	day 2	Miguel day	0	0	0	0
71-IN	367200.201	6969238.299	Tailings embankment	Cu-Au	day	Miguel day	0	0	0	0
72-IN	367474.629	6969425.527	Tailings embankment	Au	desconocido	Miguel day	0	0	0	0
73-AC	445679.639	6881608.861	Tailings embankment	Cu	arenas el tambo	minera lumina Cu chile ltda.	0.33	-	0.34	-
74-AC	438697.392	6887926.751	Dam	Cu	lamas la brea	minera lumina Cu chile ltda.	0.39	-	0.39	-
75-IN	366253.053	6967854.633	Tailings embankment	Au-Cu	tranque	minera San marino	0	0	0	0
76-IN	365983.087	6966947.31	Dam	Cu	deposito 1	minex S.A	0	0	0	0.14
77-AC	365943.233	6966923.45	Dam	Cu	deposito 2	minex S.A	0	0	0	0
78-IN	366325.592	6967579.366	Dam	Au	ojos de agua	natiman flores diaz	0	0	0	0.97
79-AC	366285.206	6967483.158	Dam	Au	ojos de agua	natiman flores diaz	0	0	0	0
80-AC	369864.080	6965606.012	Tailings embankment	Cu	tranque de relave	nelson zuñiga carvajal	0	1.60	0	2.81
81-IN	370719.921	6968108.491	Tailings embankment	Au-Cu	llaucaven 1	Nuñez hnos	0	0.41	0	0.2
82-IN	370605.740	6968224.081	Tailings embankment	Au-Cu	llaucaven 2	Nuñez hnos	0	0.20	0	0
83-IN	366920.526	6967832.389	Tailings embankment	Cu-Au-Fe	farah 1-2-3-4-5-6-7	op mining chile spa	0	0.20	0	0.17
84-IN	367103.134	6968157.537	Dam	Cu-Au	embalse op	op mining chile spa	0	0	0	0
85-IN	365667.954	6967255.184	Tailings embankment	Au	monserrat	oscar gomez escobar	0	0	0	0.2
86-IN	400243.180	6901615.261	Tailings embankment	Cu	amolanas	p.l. servicios ltda.	0.36	-	0.36	-
87-AC	367327.143	6969390.25	Dam	Au	rapelina	Pedro jesus castillo vega	0	0	0	0
89-IN	374420.615	6963175.717	Tailings embankment	Cu	Maria Isabel 2	Rodrigo Barrera Barrera (ex nelson soto)	0	-	0	-
88-IN	374419.074	6963154.575	Tailings embankment	Cu	Maria Isabel 3	Rodrigo Barrera Barrera (ex nelson soto)	0	-	0	-
91-AB	362831.382	6966482.677	Tailings embankment	Au	andacollo 1	s. Pizarro (ex rubelindo alquinta)	0.17	-	0.18	-
90-AB	362828.752	6966507.974	Tailings embankment	Au	andacollo 2	s. Pizarro (ex rubelindo alquinta)	0.17	-	0.18	-

https://doi.org/10.5194/egusphere-2022-122
Preprint. Discussion started: 11 April 2022

92-AC	374784.353	6971246.491	Tailings embankment	Cu	el gato	scm atacama kozan	0.2	3.92	0.21	4.48
93-IN	372401.368	6970993.316	Dam	Au-Cu	tranque de relave	scm San sebastian	0	0	0	0
94-IN	372665.546	6959254.075	Tailings embankment	Cu	don luis 2	scm zepolac	0.18	-	0.19	-
95-IN	369993.711	6965789.058	Dam	Cu	Candelaria 1	slm escondida una de las sierras rajo de oro	0	0	0	0
96-IN	370004.351	6965837.306	Dam	Cu	Candelaria 2	slm escondida una de las sierras rajo de oro	0	0	0	0.32
97-IN	369972.631	6965872.709	Dam	Cu	Candelaria 3	slm escondida una de las sierras rajo de oro	0	0	0	0
98-AC	369143.623	6966714.539	Tailings embankment	Cu	tranque 3	soc. contractual minera alianza	0	0.52	0	1.1
99-AC	369524.187	6966663.986	Tailings embankment	Cu	tranque 2	soc. contractual minera alianza	0.13	3.02	0.13	4.12
100-IN	369728.114	6966775.514	Tailings embankment	Au	tranque 1	soc. contractual minera alianza	0	0	0	0
101-AC	366014.631	6967648.849	Dam	Cu-Au	arcadio	soc. guerrero hermanos y CIA. ltda.	0	0	0	0
102-AC	367796.927	6969554.659	Tailings embankment	Cu	corona	soc. minera Candelaria	0	0.59	0	0.38
103-IN	367223.102	6969672.102	Tailings embankment	Cu	puerto rico 0-1-2	soc. minera fortuna ltda.	0	0.20	0	0.33
104-AC	367422.484	6969800.194	Dam	Cu	embalse 4	soc. minera fortuna ltda.	0	0	0	0
105-IN	374359.627	6963717.015	Tailings embankment	Cu-Au	san joaquin 1	soc. minera San Joaquin	0	0	0	0
106-IN	374186.500	6963848.438	Tailings embankment	Cu-Au	san joaquin 2	soc. minera San Joaquin	0.16	0	0.17	0
107-IN	374306.340	6963852.544	Tailings embankment	Cu-Au	san joaquin 3	soc. minera San Joaquin	0.16	0	0.17	0
108-AB	366644.646	6968495.59	Tailings embankment	Cu	union	soc. minera union	0	0	0	0
109-AC	369029.681	6963039.76	Tailings embankment	Cu	las cruces	soc. punta del cobre S.A	0.12	-	0.13	-
110-IN	372695.571	6959636.154	Tailings embankment	Cu	el buitre	soc. punta del cobre S.A	0	-	0	-
111-IN	373650.428	6959487.019	Tailings embankment	Cu	san jose	soc. punta del cobre S.A	0	-	0	-
112-IN	370184.661	6963103.551	Tailings embankment	Cu	las cruces 2	soc. punta del cobre S.A	0	-	0	-
113-IN	366031.264	6967555.349	Tailings embankment	Cu	tranque de relave	sotratec-minart ltda.	0	0	0	0
114-AC	365934.501	6967628.579	Dam	Cu	embalse de relave	sotratec-minart ltda.	0	0	0	0
115-IN	375149.988	6965727.395	Tailings embankment	Au	la florida 2	Victor Jensen	0	0.20	0	0.94

https://doi.org/10.5194/egusphere-2022-122
Preprint. Discussion started: 11 April 2022

116-IN	374990.632	6965880.349	Tailings embankment	Au	la florida 1	Victor Jensen	0	0.15	0	0.17
117-AC	374351.225	6964463.307	Tailings embankment	Fe	tranque de relave	zsc minerals	0	0	0	0
118-IN	374431.626	6963225.142	Tailings embankment	Cu	Maria Isabel 1	Rodrigo Barrera Barrera (ex nelson soto)	0	-	0	-

https://doi.org/10.5194/egusphere-2022-122
Preprint. Discussion started: 11 April 2022

515 **Appendix B. Sensitivity to HSR parameters of flood extent delineation obtained with the terrain-based tool for Copiapó River Basin**

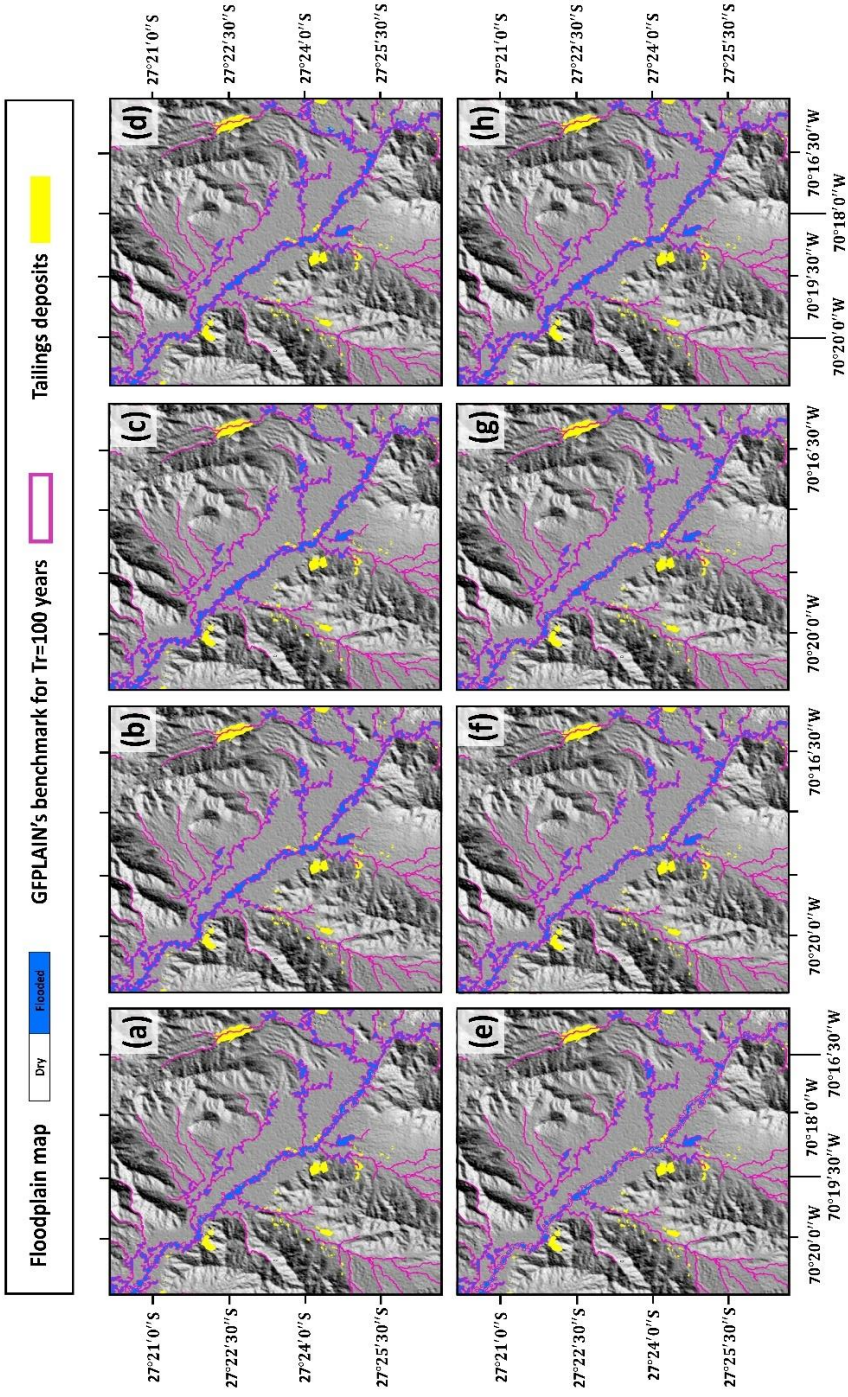

Figure B1. Sensitivity of floodplain delineation to changes in Manning's coefficient (n) **(a)** n= 0.01; **(b)** n= 0.02, **(c)** n=0.03, **(d)** n=0.05 and Sampled Stream Orders (SSO). **(e)** SSO = 1 and 2, **(f)** SSO = 2 and 3, **(g)** SSO = 3 and 4, and **(H)** SSO = 4 and 5. All floodplain maps obtained with the modified version of GFPLAIN for Tr= 100 years. All maps plotted with ALOS-Palsar RTC product (JAXA/METI-ASF, 2007) as background DEM.

https://doi.org/10.5194/egusphere-2022-122
Preprint. Discussion started: 11 April 2022

Appendix C. Flood exposure of tailings deposits inside Copiapó River Basin based on results obtained with a terrain-based floodplain mapping tool for a return period of 100 years

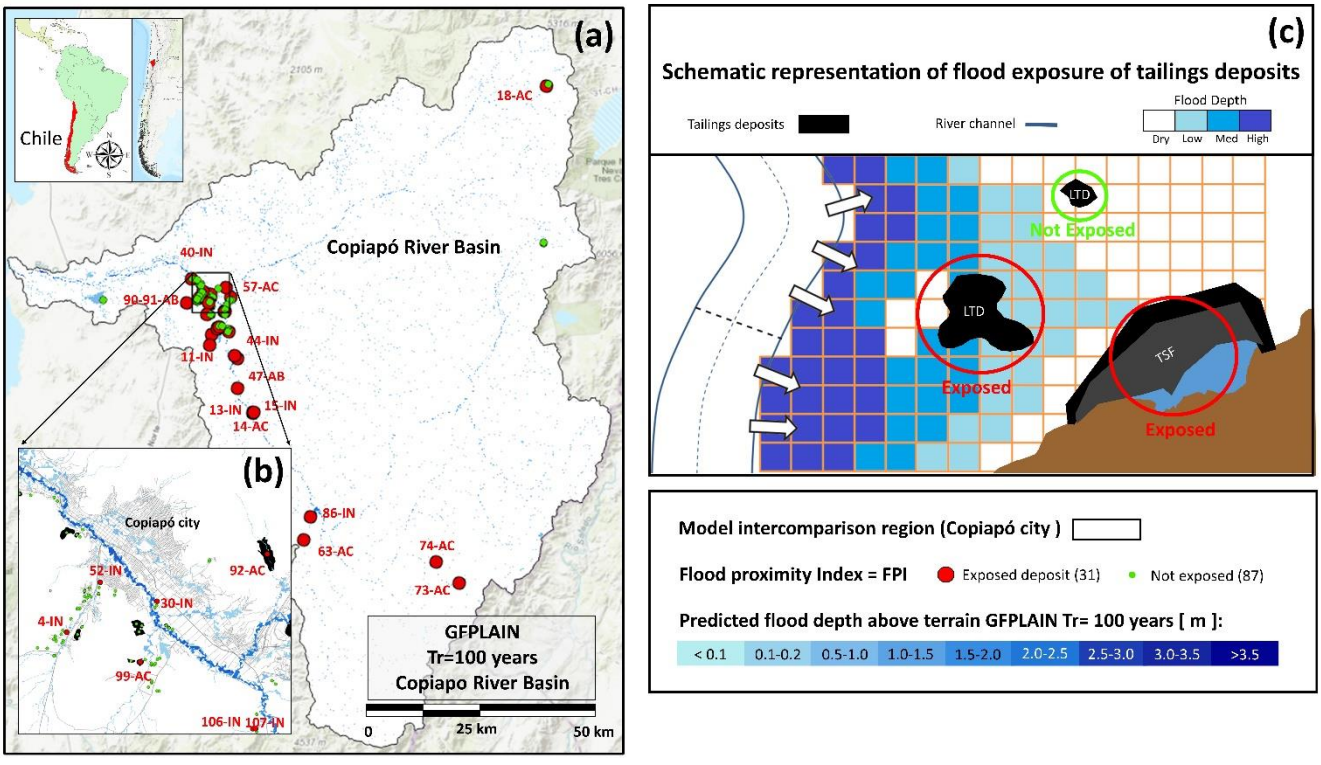

Figure C1. (a) Flood exposure of tailings deposits at a river basin scale based on the floodplain map delineated with GFPLAIN for a return period of 100 years. Background image: topographic basemap provided by Esri 2021 **(b)** Zoom to intercomparison region with 75 tailings deposits in the vicinity of Copiapó city. **(c)** Schematic representation of flood exposure assessment of Tailings Storage Facilities (TSFs) and Legacy Tailings Deposits (LTDs) using computational flood mapping tools.

https://doi.org/10.5194/egusphere-2022-122
Preprint. Discussion started: 11 April 2022

7 Authors contribution

R. C. Z. Cohen and M. Prakash performed the calibration and validation of SWIFT for flood event of March 2015. G., Pérez-Murillo implement GFPLAIN code and performed simulations for GFPLAIN and SWIFT for Tr= 100 years. G., Pérez-Murillo and N., McIntyre wrote the manuscript. R. C. Z. Cohen, N. McIntyre and M. Prakash reviewed and edited the manuscript.

8 Code availability statement

The version of GFPLAIN used in this research was modified from its original version (https://github.com/fnardi/GFPLAIN) to run under Python 3.7 using ArcGIS's python installation as interpreter (Esri, 2020). This new implementation of GFPLAIN (as Python scripts) can be download at the following repository: https://github.com/gperez1404/GFPLAIN.git. The GUI version of SWIFT can be downloaded upon request from: https://research.csiro.au/swift/download/.

9 Data availability statement

The data that support the findings of this study are available from the corresponding author upon reasonable request.

10 Competing interests

The authors declare that they have no conflict of interest

11 Acknowledgments

This research was made possible by the support and funding provided by the Sustainable Minerals Institute (SMI) and The University of Queensland's RTP scholarship. Additionally, the first author would like to thank the CSIRO, particularly the Data61 team at Clayton (Victoria), for hosting the first author during a two-month research visit in 2019. Finally, the authors thankfully acknowledge the assistance and contributions made by Dr. D. Aitken (SMI-ICE Chile) and Dr. S. Edwards (UCL, UK).

https://doi.org/10.5194/egusphere-2022-122
Preprint. Discussion started: 11 April 2022

References

Afshari, S., Tavakoly, A. A., Rajib, M. A., Zheng, X., Follum, M. L., Omranian, E., and Fekete, B. M.: Comparison of new generation low-complexity flood inundation mapping tools with a hydrodynamic model, Journal of Hydrology, 556, 539-556, https://doi.org/10.1016/j.jhydrol.2017.11.036, 2018.

Alfieri, L., Burek, P., Feyen, L., and Forzieri, G.: Global warming increases the frequency of river floods in Europe, Hydrol. Earth Syst. Sci., 19, 2247-2260, http://dx.doi.org/10.5194/hess-19-2247-2015, 2015.

Alvarez-Garreton, C., Mendoza, P. A., Boisier, J. P., Addor, N., Galleguillos, M., Zambrano-Bigiarini, M., Lara, A., Puelma, C., Cortes, G., Garreaud, R., McPhee, J., and Ayala, A.: The CAMELS-CL dataset: catchment attributes and meteorology for large sample studies – Chile dataset, Hydrol. Earth Syst. Sci., 22, 5817-5846, http://dx.doi.org/10.5194/hess-22-5817-2018 , 2018.

(ANCOLD), Australian National Committee on Large Dams. Guidelines on Dam Safety Management, https://www.ancold.org.au/?product=guidelines-on-dam-safety-management-2003, 2003.

Andrade, S., Moffett, J., and Correa, J. A.: Distribution of dissolved species and suspended particulate copper in an intertidal ecosystem affected by copper mine tailings in Northern Chile, Marine Chemistry, 101, 203-212, https://doi.org/10.1016/j.marchem.2006.03.002, 2006.

Annis, A., Nardi, F., Morrison, R. R., and Castelli, F.: Investigating hydrogeomorphic floodplain mapping performance with varying DTM resolution and stream order, Hydrological Sciences Journal, 64, 525-538, https://doi.org/10.1080/02626667.2019.1591623, 2019.

Bakatula, E. N. and Tutu, H.: Characterization and speciation modelling of cyanide in effluent from an active slimes dam. J South African Journal of Chemistry, 69, 140-147, http://dx.doi.org/10.17159/0379-4350/2016/v69a17, 2016.

Banwart, S. A., Hedin, R. S., Younger, P. L., and Hedin, R. S. Mine water: hydrology, pollution, remediation, Kluwer Academic Publishers, Springer Netherlands : Imprint: Springer, Dordrecht Boston, 2002.

Bernhofen, M. V., Whyman, C., Trigg, M. A., Sleigh, P. A., Smith, A. M., Sampson, C. C., Yamazaki, D., Ward, P. J., Rudari, R., Pappenberger, F., Dottori, F., Salamon, P., and Winsemius, H. C.: A first collective validation of global fluvial flood models for major floods in Nigeria and Mozambique, Environmental Research Letters, 13, 104007, 10.1088/1748-9326/aae014, 2018.

Blight, G.: Chapter 5 - Mine Waste: A Brief Overview of Origins, Quantities, and Methods of Storage, in: Waste, edited by: Letcher, T. M., and Vallero, D. A., Academic Press, Boston, 77-88, https://doi.org/10.1016/B978-0-12-381475-3.10005-1, 2011.

Boening, D. W.: Ecological effects, transport, and fate of mercury: a general review, Chemosphere, 40, 1335-1351, https://doi.org/10.1016/S0045-6535(99)00283-0, 2000.

https://doi.org/10.5194/egusphere-2022-122
Preprint. Discussion started: 11 April 2022

Bonifacio Fernández Larrañaga, Pablo Rengifo Oyarce, J. F. M., Gustavo Calle Vásquez, Javier Paredes, Juan Pablo Montero, and Daiber, M. P.: Análisis integrado de gestión en cuenca del río copiapó, DIRECCION GENERAL DE AGUAS (DGA), Santiago, Chile, 2011.

Carkovic B Athena, Calcagni S. Magdalena, Vega, A. S., Coquery, M., Moya, P. M., Bonilla, C. A., and Pastén, P. A.: Active and legacy mining in an arid urban environment: challenges and perspectives for Copiapó, Northern Chile, Environmental Geochemistry and Health, 38, 1001-1014, https://doi.org/10.1007/s10653-016-9793-5, 2016.

Castro-Bolinaga, C. F., Zavaleta, E. R., and Diplas, P.: A coupled modelling effort to study the fate of contaminated sediments downstream of the Coles Hill deposit, Virginia, USA, in: IAHS-AISH Proceedings and Reports, 272-280, https://doi.org/10.5194/piahs-367-272-2015, 2015.

(CDA), Canadian Dam Association. Dam Safety Guidelines, https://cda.ca/publications/cda-guidance-documents/dam-safety-publications, 2013.

Chow V. T., Maidment, D. R., and Mays, L. W.: Applied Hydrology, McGraw-Hill, New York, NY, USA, 1988.

Claro E., Rodríguez, G. B., Prakash M., Cohen R., Caroca M. L., López A., Mirza F., Hilton J., and Prats C. Modelación y análisis de inundaciones para la cuenca del río Copiapó. Modeling and Analysis Of Flooding for the Copiapó River Basin, CSIRO-Chile, Santiago de Chile, 2018.

Climate-Data.org. Climate Copiapó (chile) [website], https://en.climate-data.org/south-america/chile/iii-region-de-atacama/copiapo-2069, (last access: 6 January 2021), 2021

Clubb, F. J., Mudd, S. M., Milodowski, D. T., Valters, D. A., Slater, L. J., Hurst, M. D., and Limaye, A. B.: Geomorphometric delineation of floodplains and terraces from objectively defined topographic thresholds, Earth Surface Dynamics, 5, 369-385, 10.5194/esurf-5-369-2017, 2017.

Cohen C. H. Raymond, Hilton E. James, Hasan Khan Shahriar, Wang Yunze , and Mahesh, P.: SWIFT: a GPU based coupled hydrodynamic/hydraulic framework for urban flood prediction, Eleventh International Conference on CFD in the Minerals and Process Industries, CSIRO, Melbourne, Australia, 2015.

Concas, A., Ardau, C., Cristini, A., Zuddas, P., and Cao, G.: Mobility of heavy metals from tailings to stream waters in a mining activity contaminated site, Chemosphere, 63, 244-253, https://doi.org/10.1016/j.chemosphere.2005.08.024, 2006.

Cortés I., Ríos J., Gaete L., and Tchernitchin, A. N.: Metales pesados en muestras ambientales de la Región de Atacama. Situación postaluviones, XIV Congreso Geologico Chileno, La Serena, Chile 2015, https://biblioteca.sernageomin.cl/opac/DataFiles/14905_v3_pp_302_305.pdf ,2015

Council, E.: EU Directive of the European Parlament and of the European Council on the estimation and management of flood risks (2007/60/EU), European Council, 27–34, 2007.

(DGA), Direccion General de Aguas. Manual de calculo de crecidas y caudales mínimos en cuencas sin información fluviometrica, https://snia.mop.gob.cl/sad/FLU398.pdf,1995

(DGA), Direccion General de Aguas. Estadísticas estaciones DGA. Información Oficial Hidrometeorológica y de Calidad de

https://doi.org/10.5194/egusphere-2022-122
Preprint. Discussion started: 11 April 2022

Aguas en Línea. https://snia.mop.gob.cl/BNAConsultas/reportes, (last access: 6 January 2021), 2021

Dodov, B. and Foufoula-Georgiou, E.: Generalized hydraulic geometry: Derivation based on a multiscaling formalism, Water Resources Research, 40, https://doi.org/10.1029/2003WR002082, 2004.

Donato, D. B., Nichols, O., Possingham, H., Moore, M., Ricci, P. F., and Noller, B. N.: A critical review of the effects of gold cyanide-bearing tailings solutions on wildlife, Environment International, 33, 974-984, https://doi.org/10.1016/j.envint.2007.04.007, 2007.

Eisler, R. and Wiemeyer, S. N.: Cyanide Hazards to Plants and Animals from Gold Mining and Related Water Issues, in: Reviews of Environmental Contamination and Toxicology, edited by: Ware, G. W., Springer New York, New York, NY, 21-54, 10.1007/978-1-4419-9100-3_2, 2004.

Environmental Agency. Framework and tools for local flood risk assessment: project report (SC070059/R3), Environment Agency, Deanery Road, Bristol, BS1 9AH, 2014.

Esri, Environmental Systems Research Institute. ArcGIS Pro: Version 2.7, Release: 12-16-2020 [software], 2020.

Esri, Environmental Systems Research Institute. "World Topographic Map" [basemap]. (last access: 6 January 2021), 2021

Falcón H. M. F., Herrera, L., and Edwards, S.: Analysis of the impact of the March 2015 flood on the tailings deposits in the Copiapo valley, 4th International Seminar on Tailings Management, Santiago de Chile2017.

Fei, J.-C., Min, X.-B., Wang, Z.-X., Pang, Z.-h., Liang, Y.-J., and Ke, Y.: Health and ecological risk assessment of heavy metals pollution in an antimony mining region: a case study from South China, Environmental Science and Pollution Research, 24, 27573-27586, 10.1007/s11356-017-0310-x, 2017.

(FEMA), Federal Emergency Management Agency. The FEMA Flood Map Service Center (MSC), https://msc.fema.gov/portal/home, 2021.

Fernández, J. and Espinoza, L.: Compilación y análisis del registro histórico de remociones en masa tipo flujo en la cuenca del río copiapó, región de atacama, SERNAGEOMIN, 87, 2020.

Foulds, S. A., Brewer, P. A., Macklin, M. G., Haresign, W., Betson, R. E., and Rassner, S. M. E.: Flood-related contamination in catchments affected by historical metal mining: An unexpected and emerging hazard of climate change, Sci. Total Environ., 476-477, 165-180, https://doi.org/10.1016/j.scitotenv.2013.12.079, 2014.

Gericke, O. J. and Smithers, J. C.: Review of methods used to estimate catchment response time for the purpose of peak discharge estimation, Hydrological Sciences Journal, 59, 1935-1971, 10.1080/02626667.2013.866712, 2014.

Gonzalez, F. R., Raval, S., Taplin, R., Timms, W., and Hitch, M.: Evaluation of Impact of Potential Extreme Rainfall Events on Mining in Peru, Natural Resources Research, 28, 393-408, 10.1007/s11053-018-9396-1, 2019.

Granato, G. E.: Estimating basin lagtime and hydrograph-timing indexes used to characterize stormflows for runoff-quality analysis, 2012.

Grimalt, J. O., Ferrer, M., and Macpherson, E.: The mine tailing accident in Aznalcollar, Sci. Total Environ., 242, 3-11, https://doi.org/10.1016/S0048-9697(99)00372-1, 1999.

Hilton, J., Miller, C., Bolger, M., Hetherton, L., and Prakash, M.: An Integrated Workflow Architecture for Natural Hazards,

https://doi.org/10.5194/egusphere-2022-122
Preprint. Discussion started: 11 April 2022

Analytics and Decision Support, Environmental Software Systems. Infrastructures, Services and Applications, Cham, 2015//, 333-342, https://doi.org/10.1007/978-3-319-15994-2_33,

Huang, W., Cao, Z.-x., Qi, W.-j., Pender, G., and Zhao, K.: Full 2D hydrodynamic modelling of rainfall-induced flash floods, Journal of Mountain Science, 12, 1203-1218, 10.1007/s11629-015-3466-1, 2015.

(ICMM) International Council on Mining and Metals. Position statement on preventing catastrophic failure of tailings storage facilities,https://www.icmm.com/en-gb/about-us/member-requirements/position-statements/tailings-governance, 2016.

Izquierdo T., Abad M., and E., B.: Catastrophic flooding caused by a mudflow in the urban area of Copiapó (Atacama Desert, northern Chile), International Conference on Urban Risks, Lisbon Portugal, , 2016.

Izquierdo, T., Bonnail, E., Abad, M., Dias, M. I., Prudêncio, M. I., Marques, R., Rodríguez-Vidal, J., and Ruiz, F.: Pollution and potential risk assessment of flood sediments in the urban area of the mining Copiapó basin (Atacama Desert), Journal of South American Earth Sciences, 103, 102714, https://doi.org/10.1016/j.jsames.2020.102714, 2020.

Izquierdo, T., Abad, M., Gómez, Y., Gallardo, D., and Rodríguez-Vidal, J.: The March 2015 catastrophic flood event and its impacts in the city of Copiapó (southern Atacama Desert). An integrated analysis to mitigate future mudflow derived damages, Journal of South American Earth Sciences, 105, 102975, https://doi.org/10.1016/j.jsames.2020.102975, 2021.

Jafarzadegan, K., Merwade, V., and Saksena, S.: A geomorphic approach to 100-year floodplain mapping for the Conterminous United States, Journal of Hydrology, 561, 43-58, https://doi.org/10.1016/j.jhydrol.2018.03.061, 2018.

Jain, S. K., Mani, P., Jain, S. K., Prakash, P., Singh, V. P., Tullos, D., Kumar, S., Agarwal, S. P., and Dimri, A. P.: A Brief review of flood forecasting techniques and their applications, International Journal of River Basin Management, 16, 329-344, 10.1080/15715124.2017.1411920, 2018.

JAXA/METI and ASF: Digital Elevation Model ALOS PALSAR RTC 12.5 meters resolution [dataset], https://urs.earthdata.nasa.gov, 2007.

Johnson, A. W., Gutiérrez, M., Gouzie, D., and McAliley, L. R.: State of remediation and metal toxicity in the Tri-State Mining District, USA, Chemosphere, 144, 1132-1141, https://doi.org/10.1016/j.chemosphere.2015.09.080, 2016.

Kincey, M., Warburton, J., and Brewer, P.: Contaminated sediment flux from eroding abandoned historical metal mines: Spatial and temporal variability in geomorphological drivers, Geomorphology, 319, 199-215, https://doi.org/10.1016/j.geomorph.2018.07.026, 2018.

Kiser, T., Hansen, J., and Kennedy, B.: Impacts and Pathways of Mine Contaminants to Bull Trout (Salvelinus confluentus) in an Idaho Watershed, Archives of Environmental Contamination and Toxicology, 59, 301-311, https://doi.org/10.1007/s00244-009-9457-x, 2010.

Kossoff, D., Dubbin, W. E., Alfredsson, M., Edwards, S. J., Macklin, M. G., and Hudson-Edwards, K. A.: Mine tailings dams: Characteristics, failure, environmental impacts, and remediation, Appl. Geochem., 51, 229-245, http://dx.doi.org/10.1016/j.apgeochem.2014.09.010, 2014.

https://doi.org/10.5194/egusphere-2022-122
Preprint. Discussion started: 11 April 2022

Lam, E. J., Montofré, I. L., Álvarez, F. A., Gaete, N. F., Poblete, D. A., and Rojas, R. J.: Methodology to Prioritize Chilean Tailings Selection, According to Their Potential Risks, International Journal of Environmental Research and Public Health, 17, 3948, 2020.

Landa, E. R.: Uranium mill tailings: nuclear waste and natural laboratory for geochemical and radioecological investigations, Journal of Environmental Radioactivity, 77, 1-27, https://doi.org/10.1016/j.jenvrad.2004.01.030, 2004.

Leopold, L. B.: The hydraulic geometry of stream channels and some physiographic implications, by Luna B. Leopold and Thomas Maddock, Jr, 1953.

Liu, C.-p., Luo, C.-l., Gao, Y., Li, F.-b., Lin, L.-w., Wu, C.-a., and Li, X.-d.: Arsenic contamination and potential health risk implications at an abandoned tungsten mine, southern China, Environmental Pollution, 158, 820-826, https://doi.org/10.1016/j.envpol.2009.09.029, 2010.

Lottermoser, B.: Mine Wastes: Characterization, Treatment and Environmental Impacts, 1-400 pp.2010.

Martín Duque José F, Zapico Ignacio , Oyarzun Roberto , López García José A. , Higueras Pablo , and Javier, L.: Environmental hazards related to abandoned mine tailings: understanding problems and seeking solutions from a geomorphic and geochemical approach, XIV Congreso Geologico Chileno, 2015.

McMaster, K.: Effects of digital elevation model resolution on derived stream network positions, J Water Resources Research, 38, 13-11-13-18, https://doi.org/10.1029/2000WR000150, 2002.

Merz, B., Aerts, J., Arnbjerg-Nielsen, K., Baldi, M., Becker, A., Bichet, A., Blöschl, G., Bouwer, L. M., Brauer, A., Cioffi, F., Delgado, J. M., Gocht, M., Guzzetti, F., Harrigan, S., Hirschboeck, K., Kilsby, C., Kron, W., Kwon, H. H., Lall, U., Merz, R., Nissen, K., Salvatti, P., Swierczynski, T., Ulbrich, U., Viglione, A., Ward, P. J., Weiler, M., Wilhelm, B., and Nied, M.: Floods and climate: emerging perspectives for flood risk assessment and management, Nat. Hazards Earth Syst. Sci., 14, 1921-1942, 10.5194/nhess-14-1921-2014, 2014.

Mhlongo, S. E., Amponsah-Dacosta, F., and Kadyamatimba, A.: Development and application of a methodological tool for prioritization of rehabilitation of abandoned tailings dumps in the Giyani and Musina areas of South Africa, Cogent Engineering, 6, 1619894, 10.1080/23311916.2019.1619894, 2019.

Mileusnić, M., Mapani, B. S., Kamona, A. F., Ružičić, S., Mapaure, I., and Chimwamurombe, P. M.: Assessment of agricultural soil contamination by potentially toxic metals dispersed from improperly disposed tailings, Kombat mine, Namibia, J. Geochem. Explor., 144, 409-420, https://doi.org/10.1016/j.gexplo.2014.01.009, 2014.

Mineria, M. d.: Decreto supremo Nº 248, reglamento para la aprobación de proyectos de diseño, construcción, operación y cierre de los depósitos de relaves, 2007.

Mitchell, I., Hryczyszyn, K., and Read, T.: A framework to prioritise high-risk abandoned mine features for rehabilitation in Western Australia, 13th International Conference on Mine Closure, Perth, 2019/09/032019.

Motevalli, A. and Vafakhah, M.: Flood hazard mapping using synthesis hydraulic and geomorphic properties at watershed scale, Stochastic Environmental Research and Risk Assessment, 30, 1889-1900, 10.1007/s00477-016-1305-8, 2016.

Nardi, F., Vivoni, E. R., and Grimaldi, S.: Investigating a floodplain scaling relation using a hydrogeomorphic delineation

https://doi.org/10.5194/egusphere-2022-122
Preprint. Discussion started: 11 April 2022

715 method, Water Resources Research, 42, https://doi.org/10.1029/2005wr004155, 2006.

Nardi, F., Annis, A., Baldassarre, G. D., Vivoni, E. R., and Grimaldi, S.: GFPLAIN250m, a global high-resolution dataset of earth's floodplains, Sci. Data, 6, 10.1038/sdata.2018.309, 2019.

Nardi, F., Biscarini, C., Di Francesco, S., Manciola, P., and Ubertini, L.: Comparing a large-scale dem-based floodplain delineation algorithm with standard flood maps: The tiber river basin case study, Irrig. Drain., 62, 11-19,
720 https://doi.org/10.1002/ird.1818, 2013.

Navarro, M. C., Pérez-Sirvent, C., Martínez-Sánchez, M. J., Vidal, J., Tovar, P. J., and Bech, J.: Abandoned mine sites as a source of contamination by heavy metals: A case study in a semi-arid zone, J. Geochem. Explor., 96, 183-193, https://doi.org/10.1016/j.gexplo.2007.04.011, 2008.

Ngole-Jeme, V. M. and Fantke, P.: Ecological and human health risks associated with abandoned gold mine tailings
725 contaminated soil, PLOS ONE, 12, e0172517, 10.1371/journal.pone.0172517, 2017.

Ngula Niipele, J. and Chen, J.: The usefulness of alos-palsar dem data for drainage extraction in semi-arid environments in The Iishana sub-basin, Journal of Hydrology: Regional Studies, 21, 57-67, https://doi.org/10.1016/j.ejrh.2018.11.003, 2019.

Ni, Y., Cao, Z., Liu, Q., and Liu, Q.: A 2D hydrodynamic model for shallow water flows with significant infiltration losses,
730 Hydrol. Processes, 34, 2263-2280, https://doi.org/10.1002/hyp.13722, 2020.

Nikolakopoulos, K. G., Choussiafis, C., and Karathanassi, V.: Assessing the quality of DSM from ALOS optical and radar data for automatic drainage extraction, Earth Science Informatics, 8, 293-307, 10.1007/s12145-014-0199-6, 2015.

Nkwunonwo, U. C., Whitworth, M., and Baily, B.: A review of the current status of flood modelling for urban flood risk management in the developing countries, Scientific African, 7, e00269, https://doi.org/10.1016/j.sciaf.2020.e00269,
735 2020.

Northey, S. A., Mudd, G. M., Werner, T. T., Jowitt, S. M., Haque, N., Yellishetty, M., and Weng, Z.: The exposure of global base metal resources to water criticality, scarcity and climate change, Global Environmental Change, 44, 109-124, https://doi.org/10.1016/j.gloenvcha.2017.04.004, 2017.

Nriagu, J. O., Wong, H. K. T., Lawson, G., and Daniel, P.: Saturation of ecosystems with toxic metals in Sudbury basin,
740 Ontario, Canada, Sci. Total Environ., 223, 99-117, https://doi.org/10.1016/S0048-9697(98)00284-8, 1998.

(ODEPA) Oficina de Estudios y Políticas Agrarias. Región de Atacama. Información Regional, actualización Junio 2019. Ministerio de Agricultura, Chile. https://www.odepa.gob.cl/wp-content/uploads/2019/06/Atacama.pdf, 2019.

Pavlowsky, R. T., Lecce, S. A., Owen, M. R., and Martin, D. J.: Legacy sediment, lead, and zinc storage in channel and floodplain deposits of the Big River, Old Lead Belt Mining District, Missouri, USA, Geomorphology, 299, 54-75,
745 https://doi.org/10.1016/j.geomorph.2017.08.042, 2017.

Pearce, T. D., Ford, J. D., Prno, J., Duerden, F., Pittman, J., Beaumier, M., Berrang-Ford, L., and Smit, B.: Climate change and mining in Canada, Mitigation and Adaptation Strategies for Global Change, 16, 347-368, 10.1007/s11027-010-9269-3, 2011.

https://doi.org/10.5194/egusphere-2022-122
Preprint. Discussion started: 11 April 2022

Prakash, M., Hilton, J., and Ramachandran, L.: Integrating Hydrodynamic and Hydraulic Modeling for Evaluating Future Flood Mitigation in Urban Environments, Environmental Software Systems. Infrastructures, Services and Applications, Cham, 2015//, 282-292,

Raymond Cohen, J. H. a. M. P.: Benchmark testing the Swift flood modelling solver: Version, CSIRO, 2016.

S. Néelz and Pender, G.: Benchmarking the latest generation of 2D hydraulic modelling packages, Environment Agency of the UK (UKEA), 2013.

Samela, C., Albano, R., Sole, A., and Manfreda, S.: A GIS tool for cost-effective delineation of flood-prone areas, Computers, Environment and Urban Systems, 70, 43-52, https://doi.org/10.1016/j.compenvurbsys.2018.01.013, 2018.

Sampson, C. C., Smith, A. M., Bates, P. D., Neal, J. C., Alfieri, L., and Freer, J. E.: A high-resolution global flood hazard model, Water Resources Research, 51, 7358-7381, https://doi.org/10.1002/2015WR016954, 2015.

Sarricolea, P., Herrera-Ossandon, M., and Meseguer-Ruiz, Ó.: Climatic regionalisation of continental Chile, Journal of Maps, 13, 66-73, 10.1080/17445647.2016.1259592, 2017.

Schanze, J.: FLOOD RISK MANAGEMENT – A BASIC FRAMEWORK, Flood Risk Management: Hazards, Vulnerability and Mitigation Measures, Dordrecht, 2006//, 1-20,

(SERNAGEOMIN), Servicio Nacional de Geología y Mineria. National registry of Tailings Storage Facilities in Chile. Oficina de depósitos de relaves, Ministerio de Mineria [dataset], https://www.sernageomin.cl/datos-publicos-deposito-de-relaves/, 2020.

Sharma, V. and Franks, D. M.: In Situ Adaptation to Climatic Change: Mineral Industry Responses to Extreme Flooding Events in Queensland, Australia, Society & Natural Resources, 26, 1252-1267, https://doi.org/10.1080/08941920.2013.797528 , 2013

Shawky, M., Moussa, A., Hassan, Q. K., and El-Sheimy, N. Pixel-Based Geometric Assessment of Channel Networks/Orders Derived from Global Spaceborne Digital Elevation Models, Remote Sensing, 11, https://doi.org/10.3390/rs11030235 , 2019.

Stephens, E., Schumann, G., and Bates, P.: Problems with binary pattern measures for flood model evaluation, 28, 4928-4937, https://doi.org/10.1002/hyp.9979, 2014.

Tabari, H.: Climate change impact on flood and extreme precipitation increases with water availability, Scientific Reports, 10, 13768, https://doi.org/10.1038/s41598-020-70816-2, 2020.

Teng, J., Jakeman, A. J., Vaze, J., Croke, B. F. W., Dutta, D., and Kim, S.: Flood inundation modelling: A review of methods, recent advances and uncertainty analysis, Environmental Modelling & Software, 90, 201-216, https://doi.org/10.1016/j.envsoft.2017.01.006, 2017.

Tügel, F., Özgen-Xian, I., Marafini, E., Hadidi, A., and Hinkelmann, R.: Flash flood simulations for an Egyptian city - mitigation measures and impact of infiltration, Urban Water Journal, 17, 396-406, https://doi.org/10.1080/1573062X.2020.1713171, 2020.

Valdés-Pineda, R., Valdes, J., and Garcia-Chevesich, P.: Mudflow Modeling in the Copiapó Basin, Chile, 135-152 pp.,

https://doi.org/10.5194/egusphere-2022-122
Preprint. Discussion started: 11 April 2022

https://doi.org/10.4995/ia.2017.7366, 2017.

White, B., Ogilvie, J., Campbell, D. M. H. M. H., Hiltz, D., Gauthier, B., Chisholm, H. K. H., Wen, H. K., Murphy, P. N. C. N. C., and Arp, P. A. A.: Using the Cartographic Depth-to-Water Index to Locate Small Streams and Associated Wet Areas across Landscapes, Canadian Water Resources Journal / Revue canadienne des ressources hydriques, 37, 333-347, 10.4296/cwrj2011-909, 2012.

Winde, F. and Jacobus van der Walt, I.: The significance of groundwater–stream interactions and fluctuating stream chemistry on waterborne uranium contamination of streams—a case study from a gold mining site in South Africa, Journal of Hydrology, 287, 178-196, https://doi.org/10.1016/j.jhydrol.2003.10.004, 2004.

Wing, O. E. J., Bates, P. D., Sampson, C. C., Smith, A. M., Johnson, K. A., and Erickson, T. A.: Validation of a 30 m resolution flood hazard model of the conterminous United States, 53, 7968-7986, https://doi.org/10.1002/2017WR020917, 2017.

Zhao, Y., Feng, D., Yu, L., Wang, X., Chen, Y., Bai, Y., Hernández, H. J., Galleguillos, M., Estades, C., Biging, G. S., Radke, J. D., and Gong, P.: Detailed dynamic land cover mapping of Chile: Accuracy improvement by integrating multi-temporal data, Remote Sensing of Environment, 183, 170-185, https://doi.org/10.1016/j.rse.2016.05.016, 2016.

Zheng, X., Maidment, D. R., Tarboton, D. G., Liu, Y. Y., and Passalacqua, P.: GeoFlood: Large-Scale Flood Inundation Mapping Based on High-Resolution Terrain Analysis, 54, 10,013-010,033, https://doi.org/10.1029/2018WR023457, 2018.